Electronic Supporting Information

Investigation of the Role of Hydrogen Bonding in Ionic Liquid-like Salts with both N- and S-Soft Donors

Olivier Renier,[a] Guillaume Bousrez,[a] Volodymyr Smetana,[a] Anja-Verena Mudring,*[a,b] Robin D. Rogers*[c]

[a]Department of Materials and Environmental Chemistry, Stockholm University, 10691 Stockholm, Sweden.

[b]Department of Chemistry and iNANO, 253 Aarhus University, 8000 Aarhus C, Denmark

[c]Department of Chemistry & Biochemistry , The University of Alabama, Tuscaloosa, AL 35487, USA.

Table of Contents:

I. ^{1}H and ^{13}C NMR spectra for 1-6

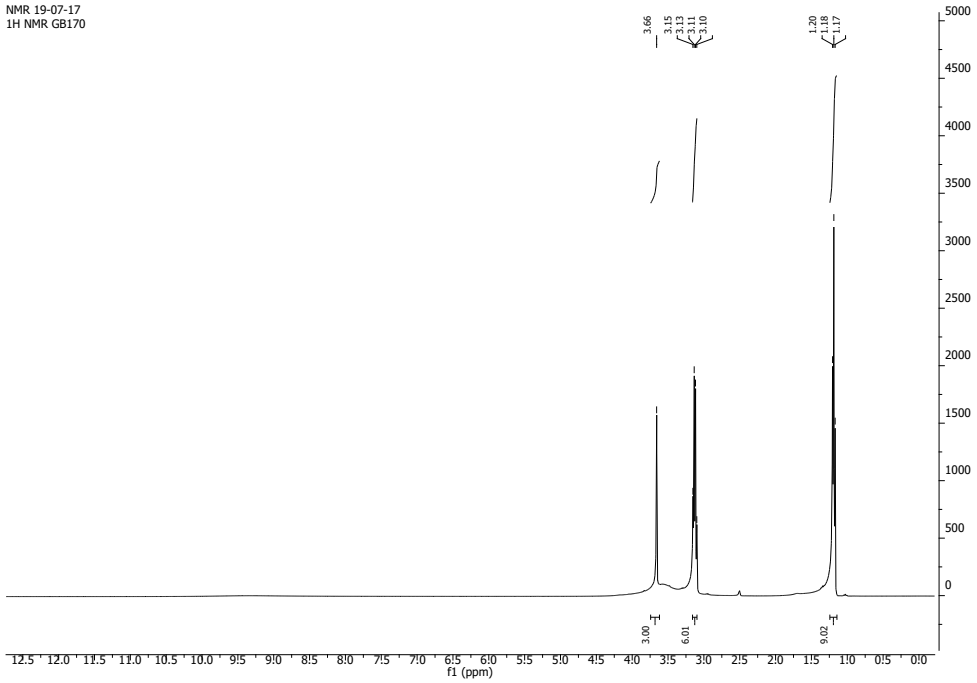

Figure S1: ^{1}H-NMR spectrum (400 MHz, DMSO-d_6) of **1**.

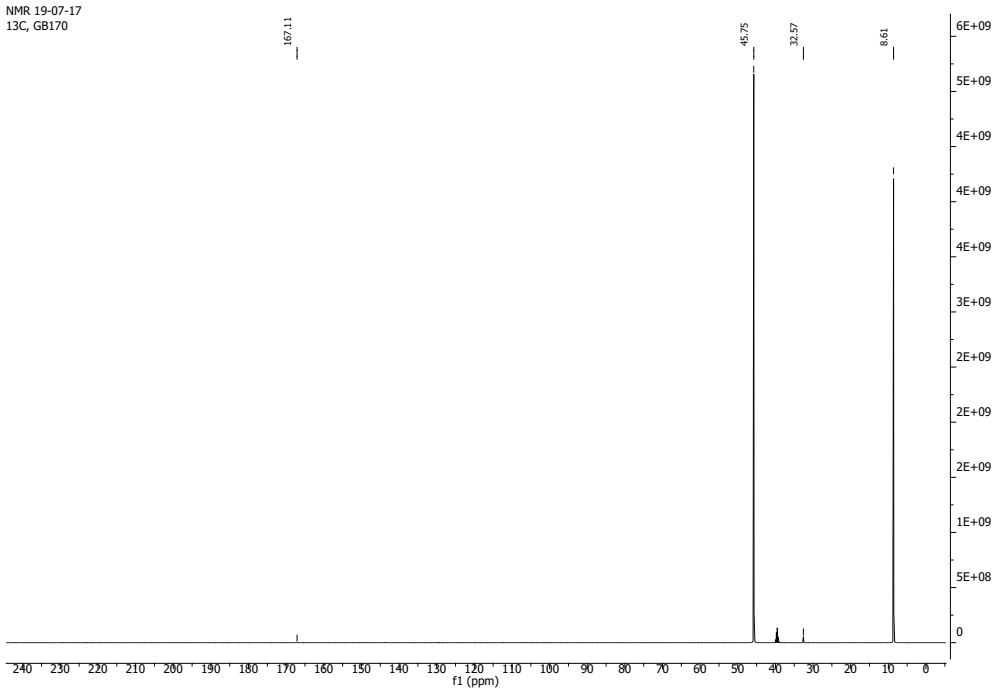

Figure S2: ^{13}C-NMR spectrum (100 MHz, DMSO-d_6) of **1**.

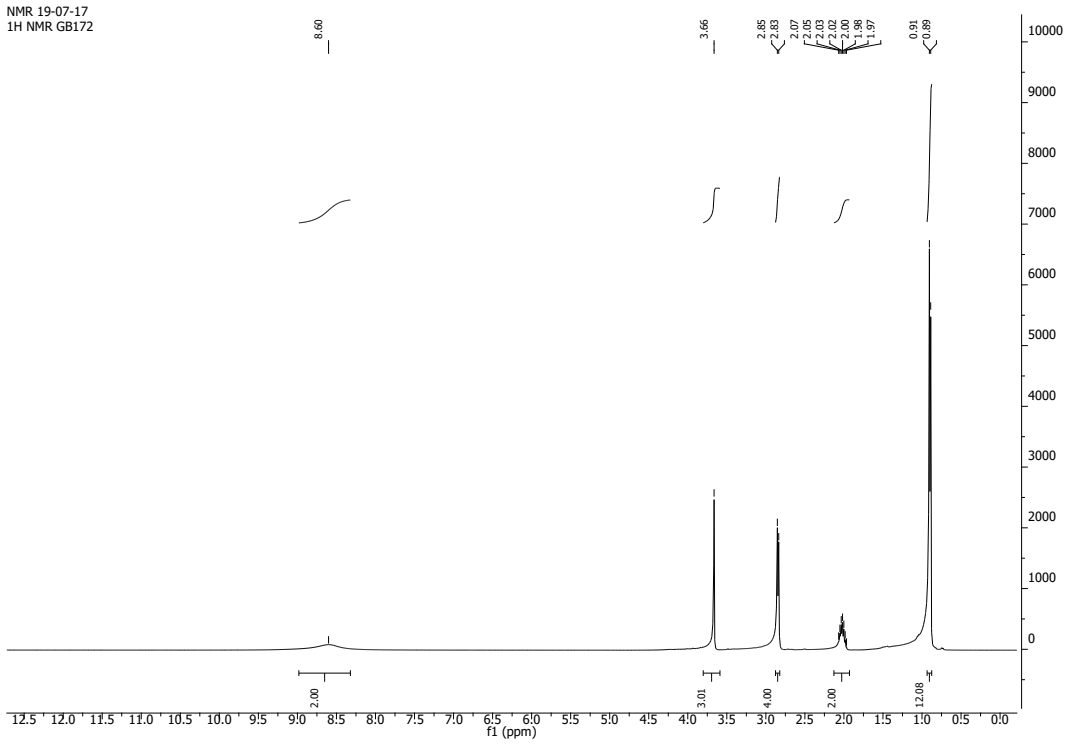

Figure S3: ^{1}H-NMR spectrum (400 MHz, DMSO-d_6) of **2**.

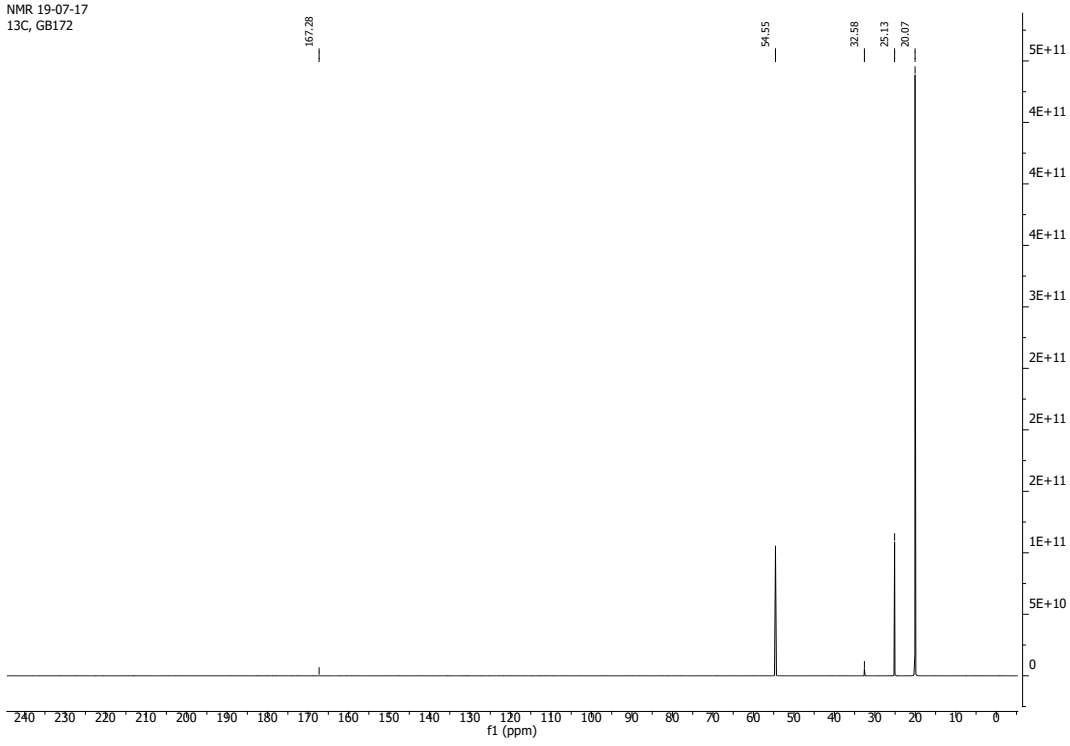

Figure S4: ^{13}C-NMR spectrum (100 MHz, DMSO-d_6) of **2**.

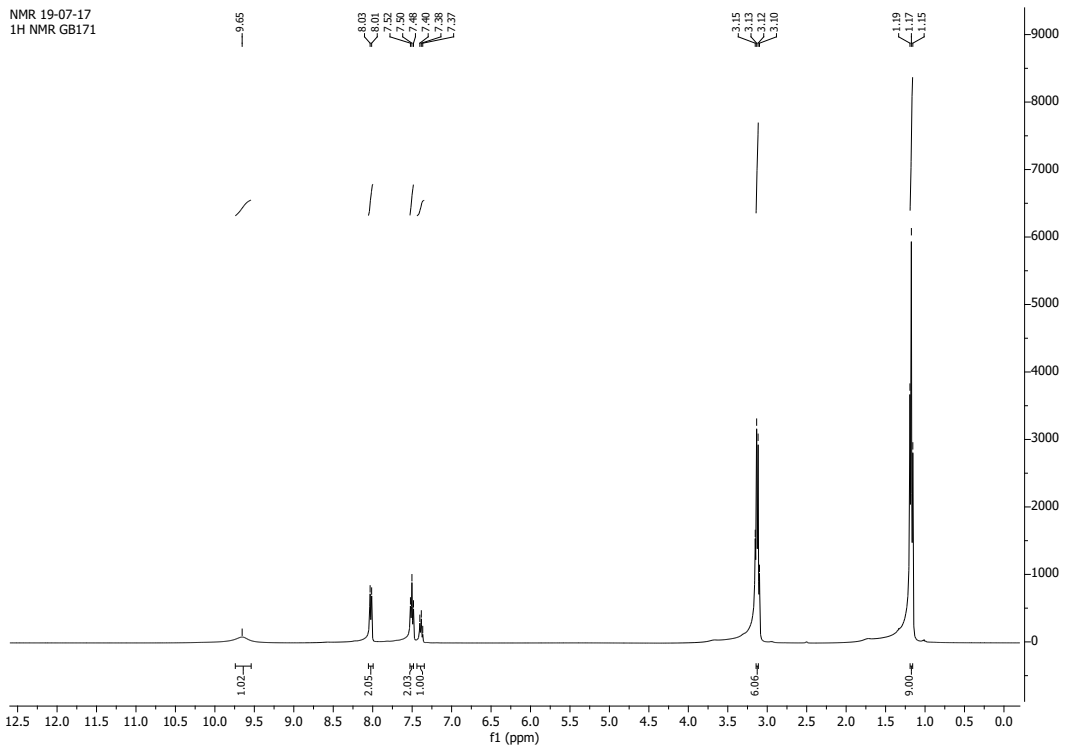

Figure S5: ^{1}H-NMR spectrum (400 MHz, DMSO-d_6) of **3**.

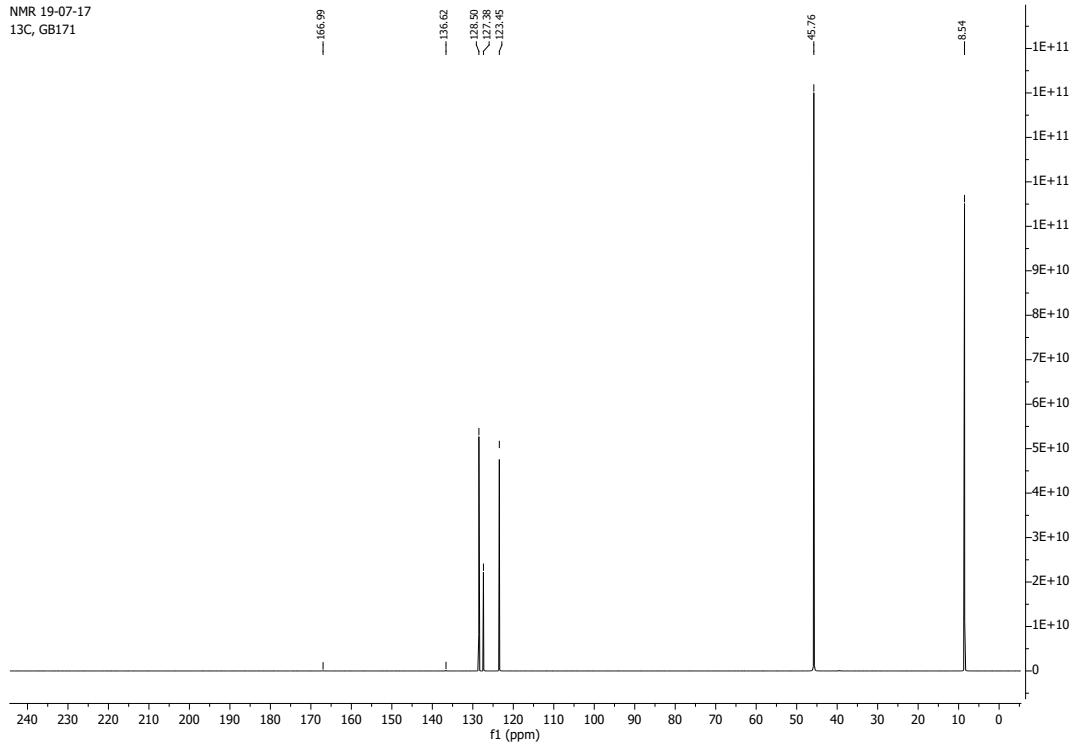

Figure S6: ^{13}C-NMR spectrum (100 MHz, DMSO-d_6) of **3**.

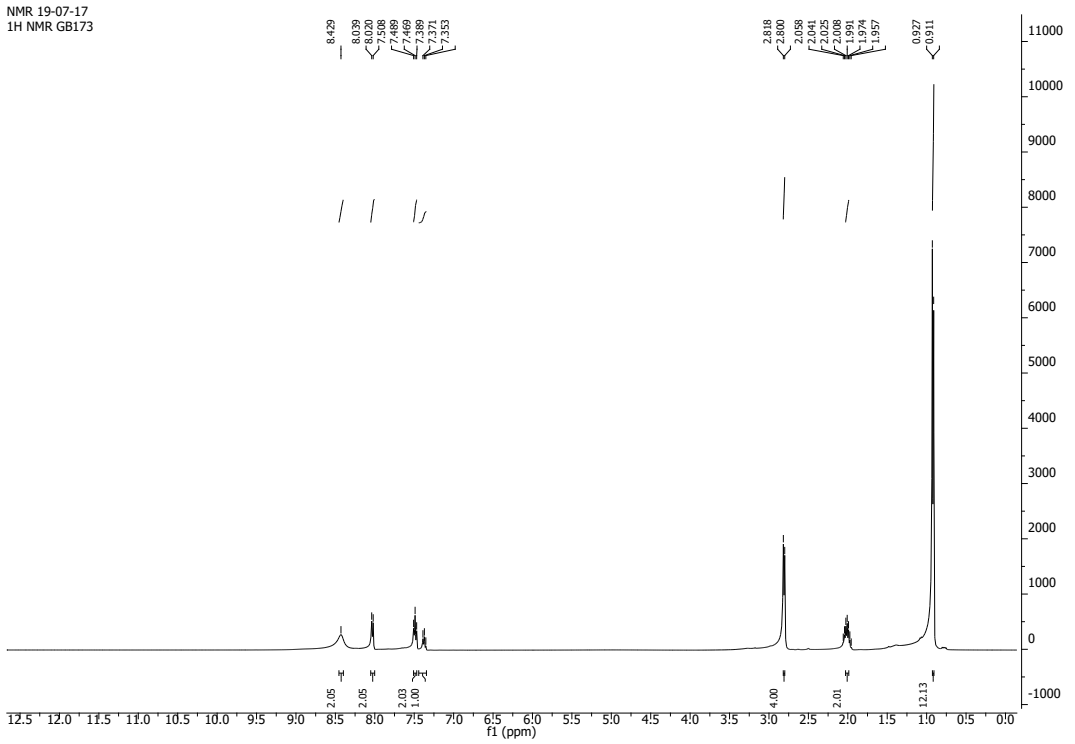

Figure S7: ^{1}H-NMR spectrum (400 MHz, DMSO-d_6) of **4**.

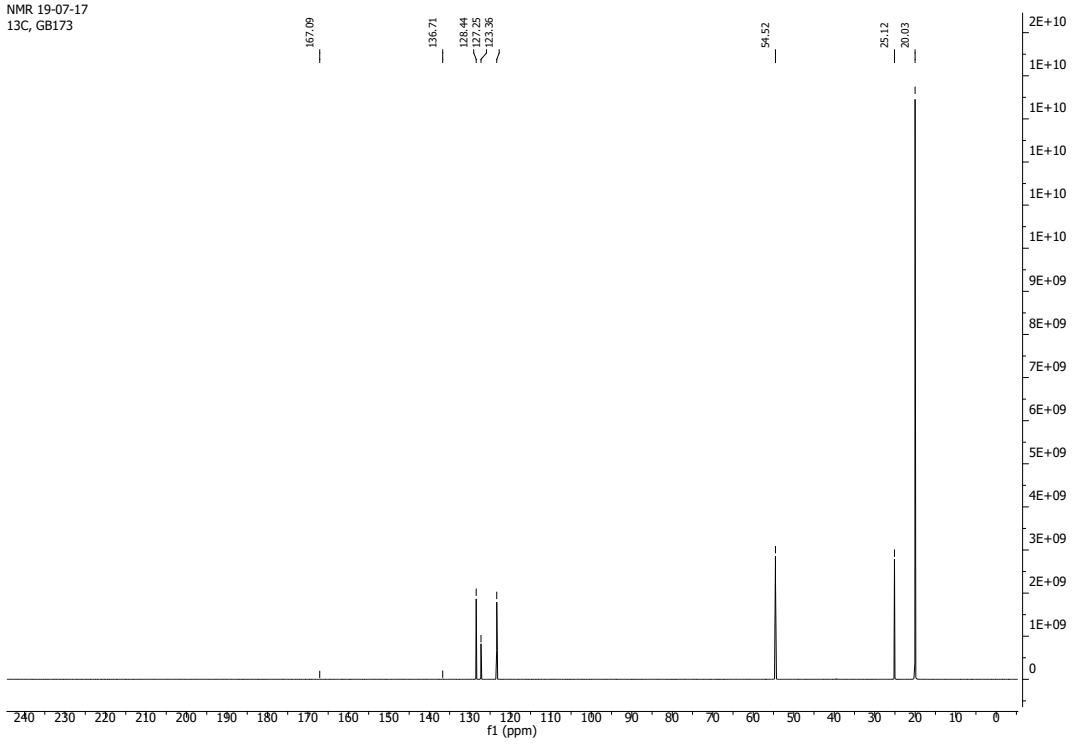

Figure S8: ^{13}C-NMR spectrum (100 MHz, DMSO-d_6) of **4**.

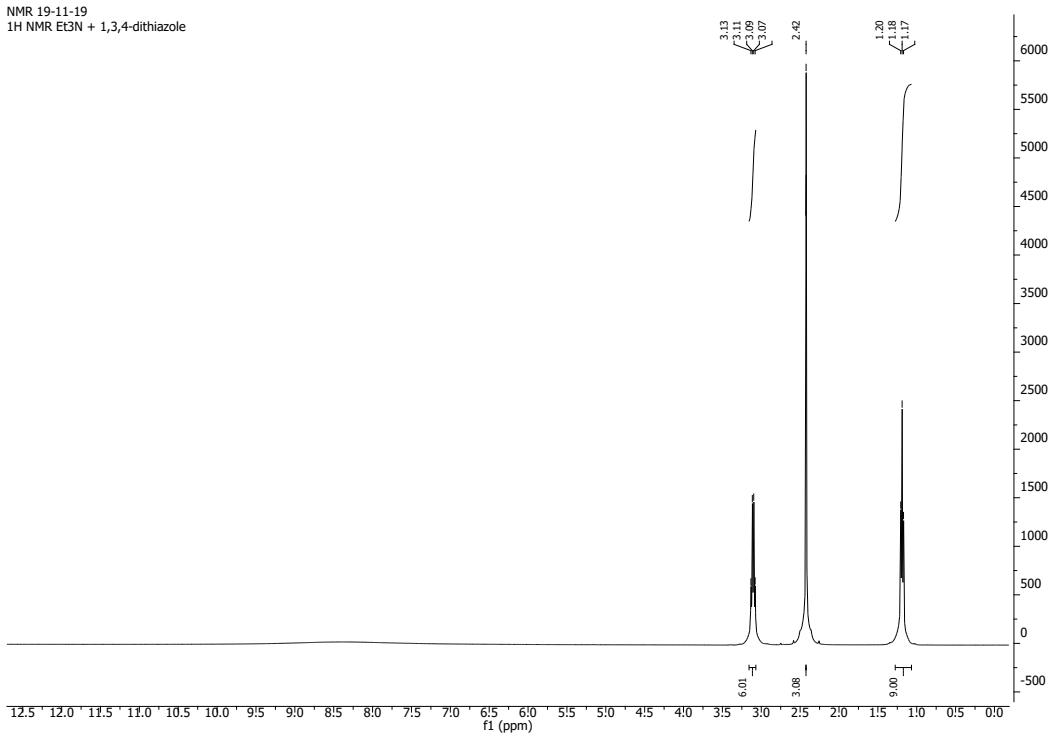

Figure S9: ^{1}H-NMR spectrum (400 MHz, DMSO-d_6) of **5**.

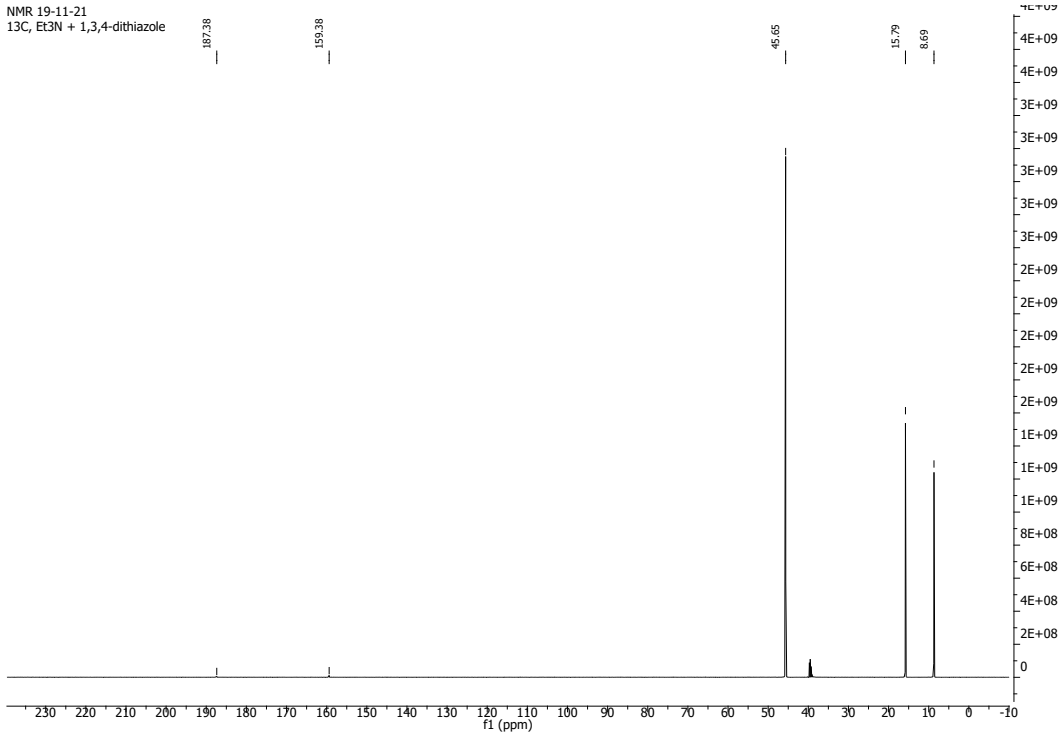

Figure S10: ^{13}C-NMR spectrum (100 MHz, DMSO-d_6) of **5**.

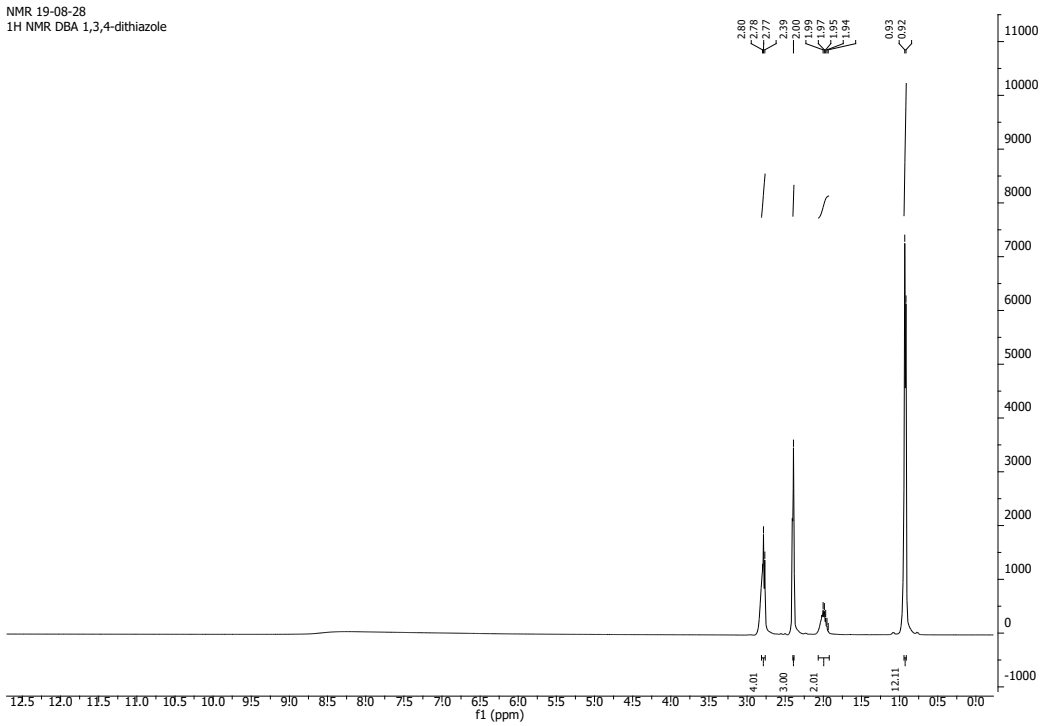

Figure S11: ^{1}H-NMR spectrum (400 MHz, DMSO-d_6) of **6**.

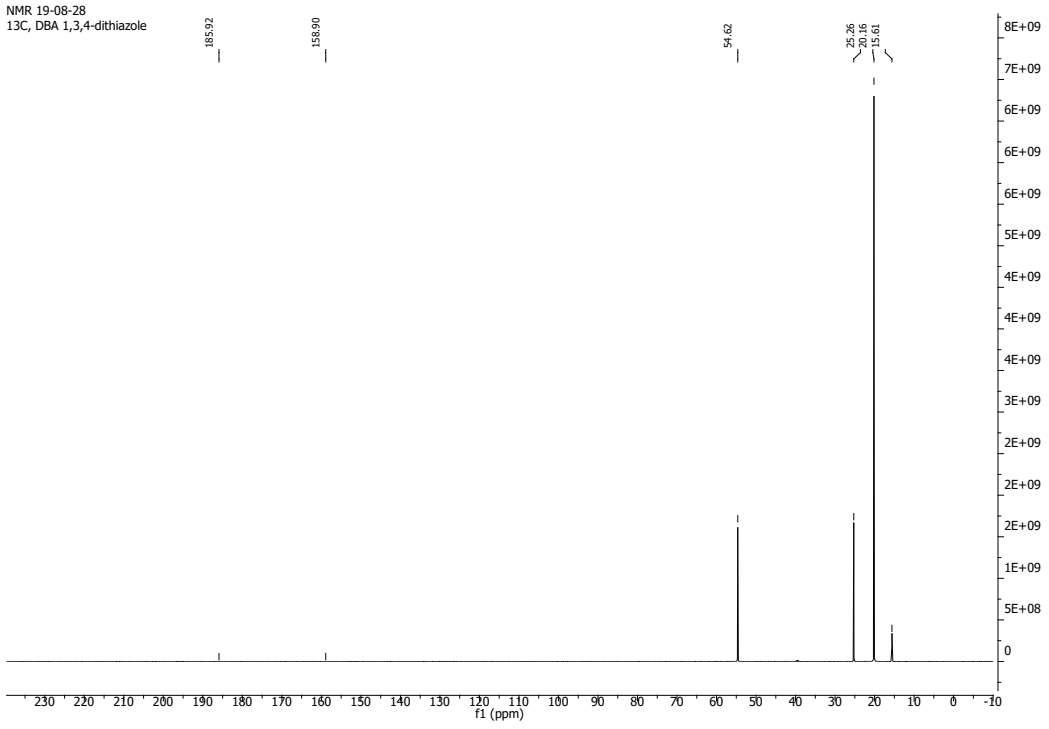

Figure S12: ^{13}C-NMR spectrum (100 MHz, DMSO-d_6) of **6**.

II. Infrared spectra for 1-6

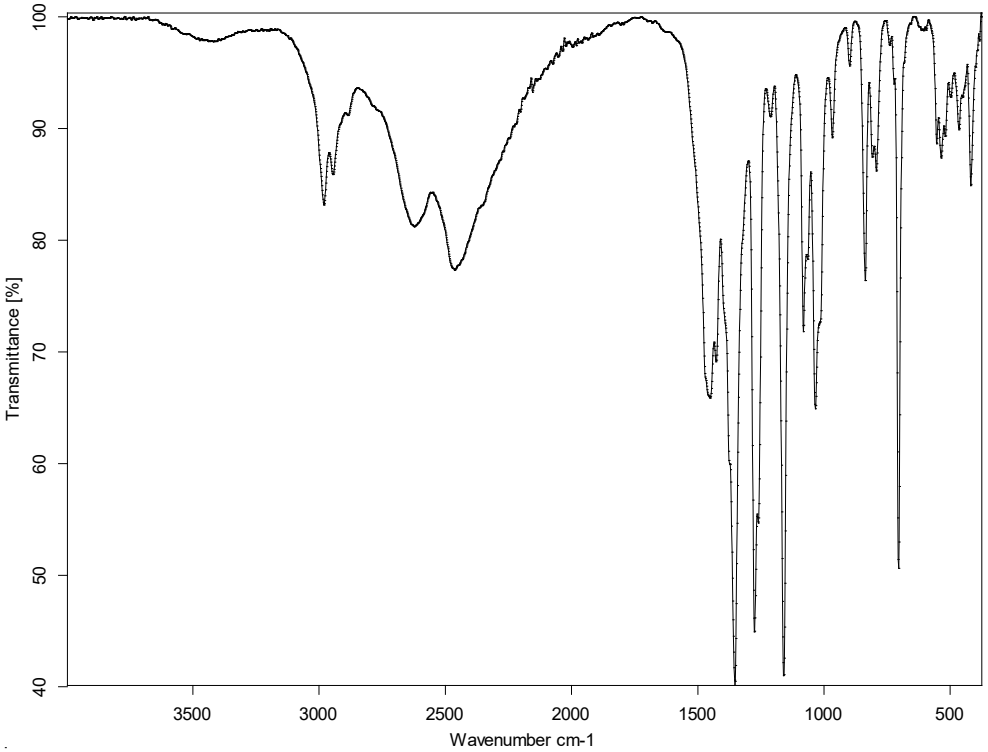

Figure S13: Infrared spectrum of **1**.

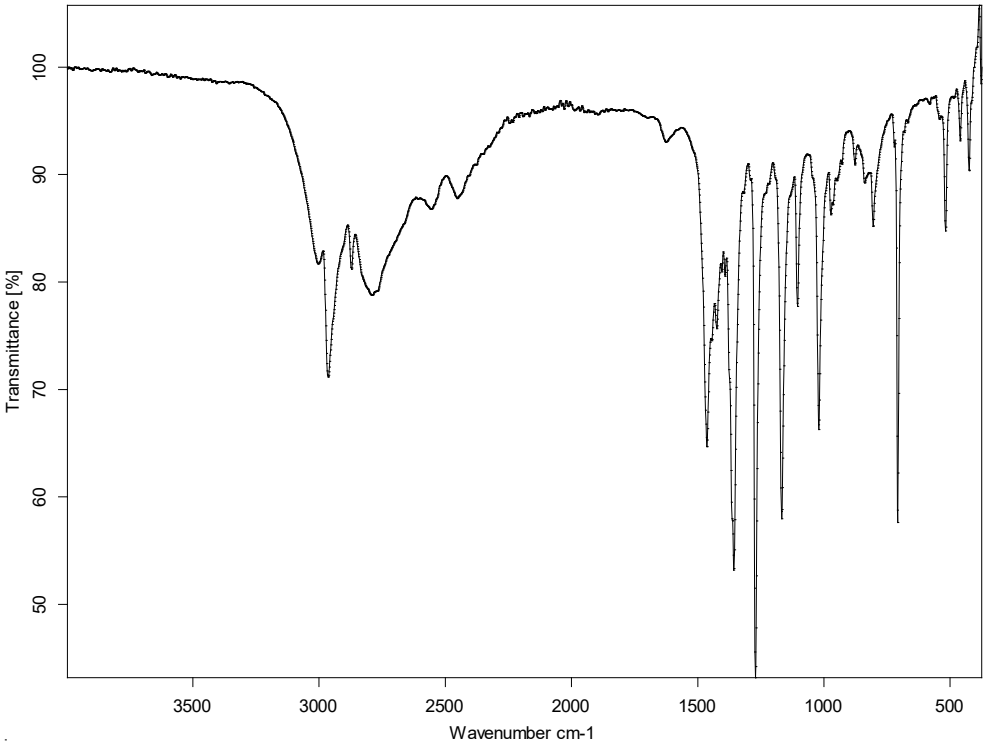

Figure S14: Infrared spectrum of **2**.

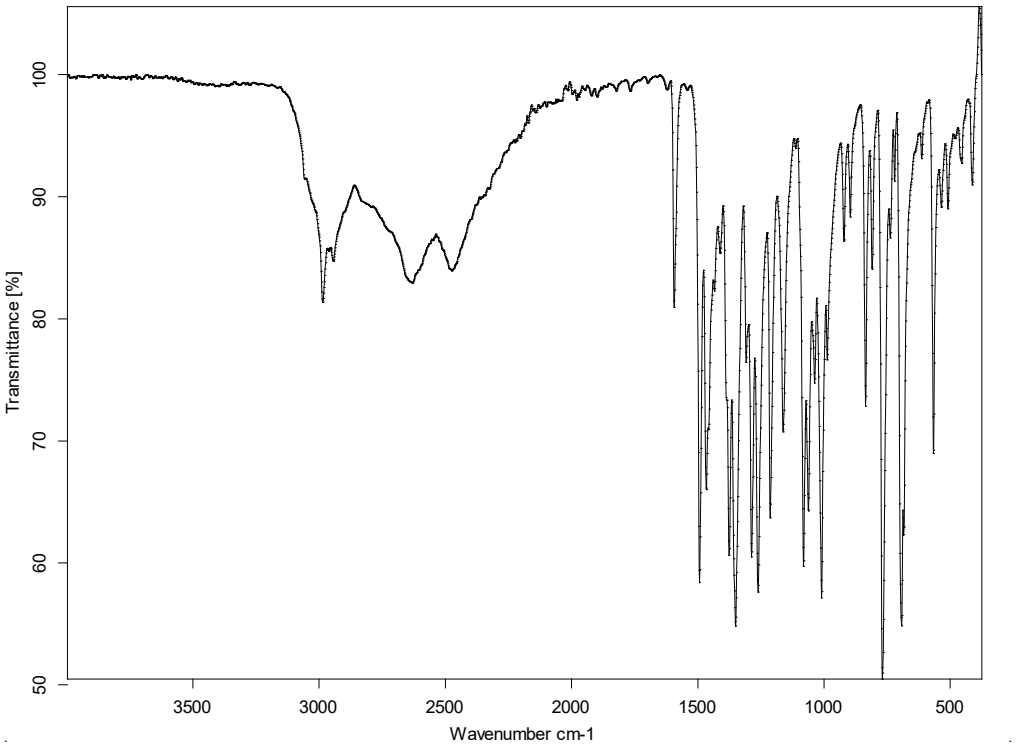

Figure S15: Infrared spectrum of **3**.

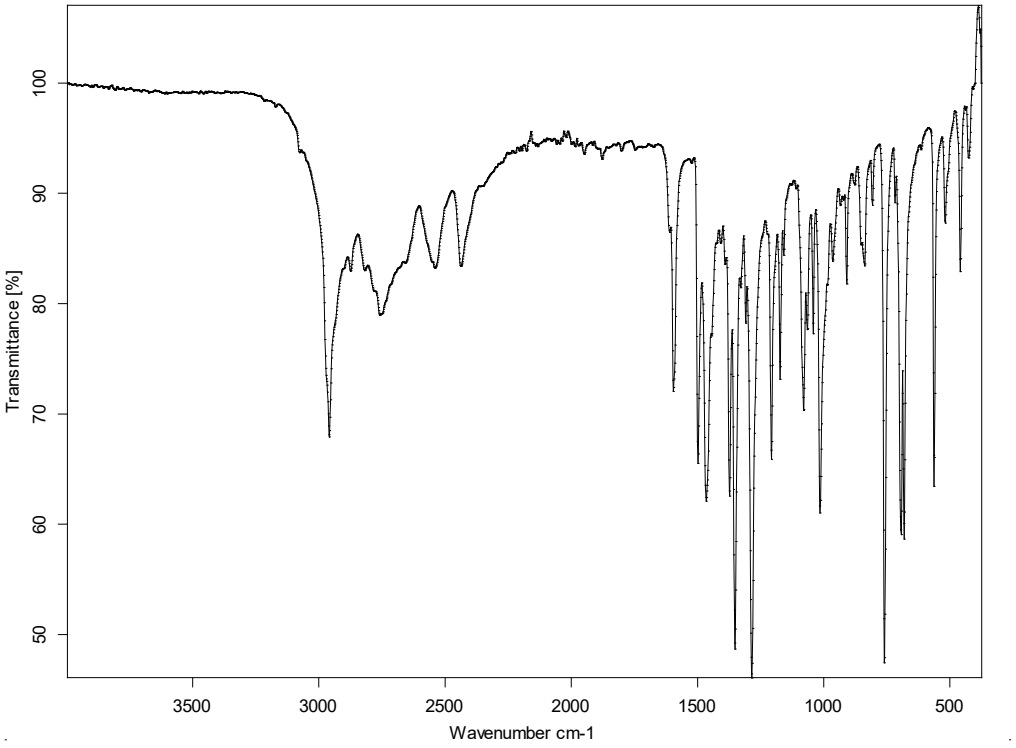

Figure S16: Infrared spectrum of **4**.

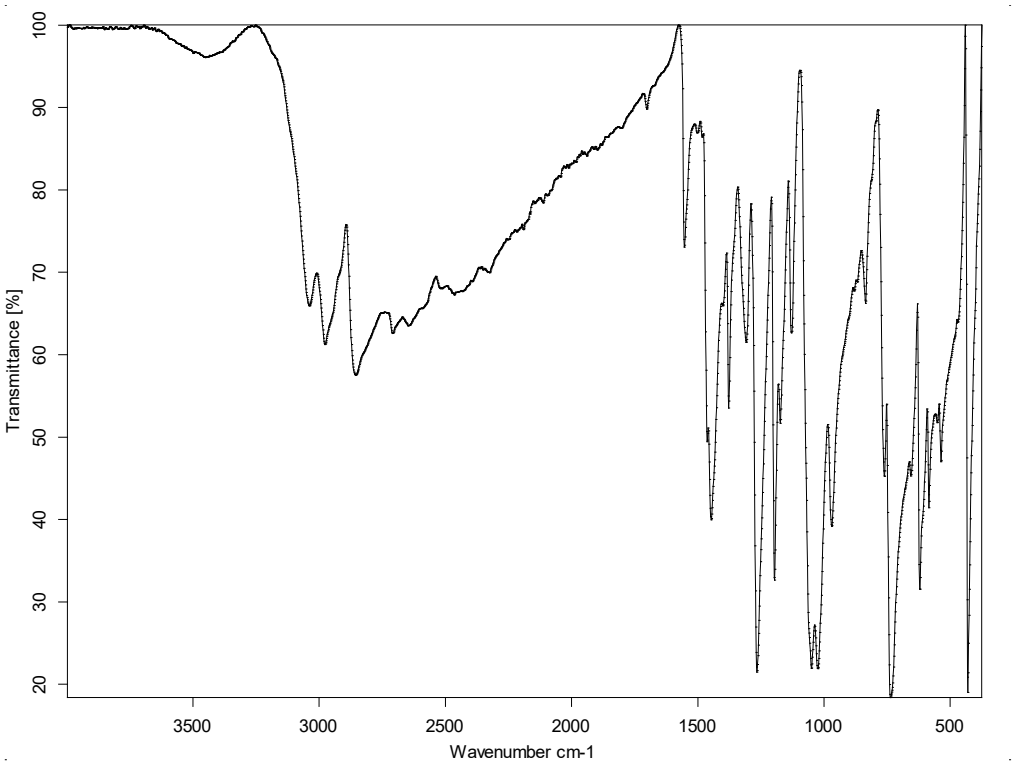

Figure S17: Infrared spectrum of **5**.

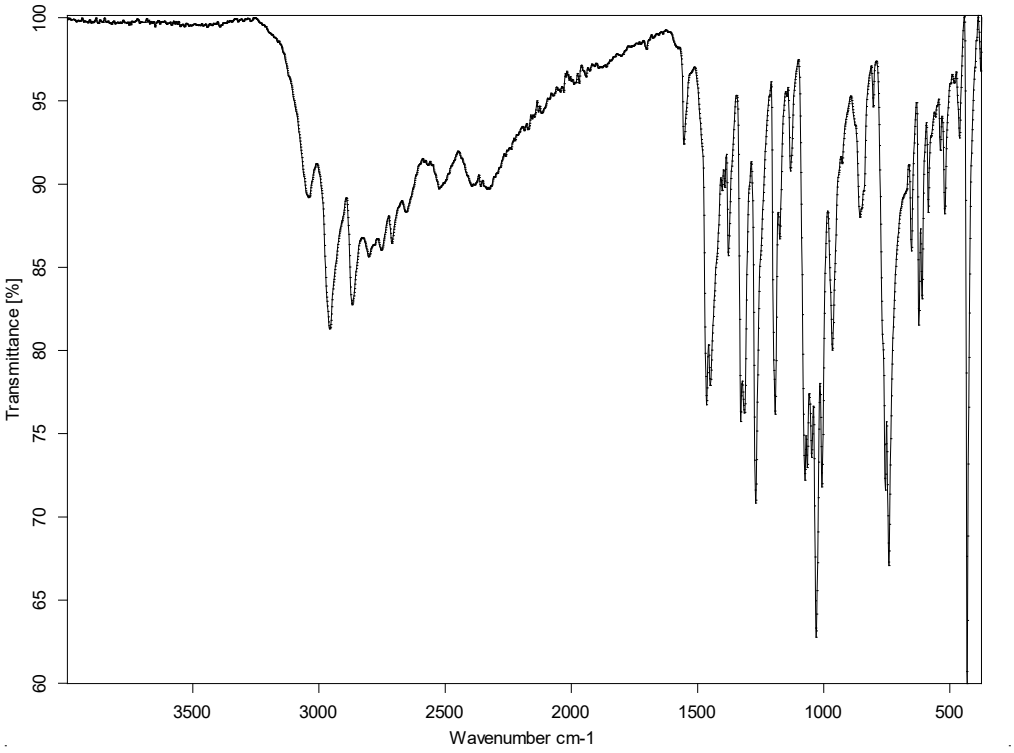

Figure S18: Infrared spectrum of **6**.

III. Differential Scanning Calorimetry (DSC) traces for 1-6

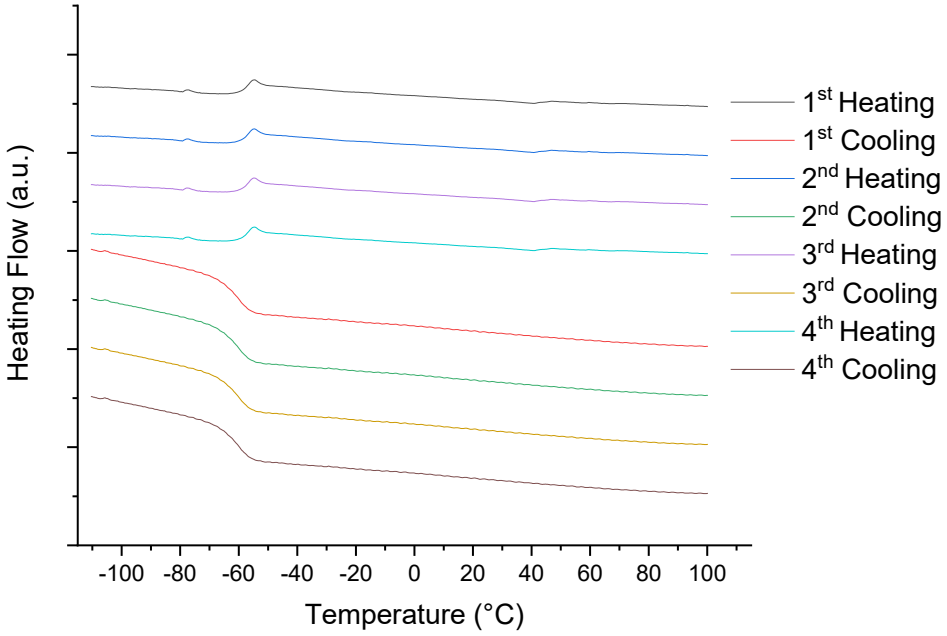

Figure S19: DSC traces of **1**.

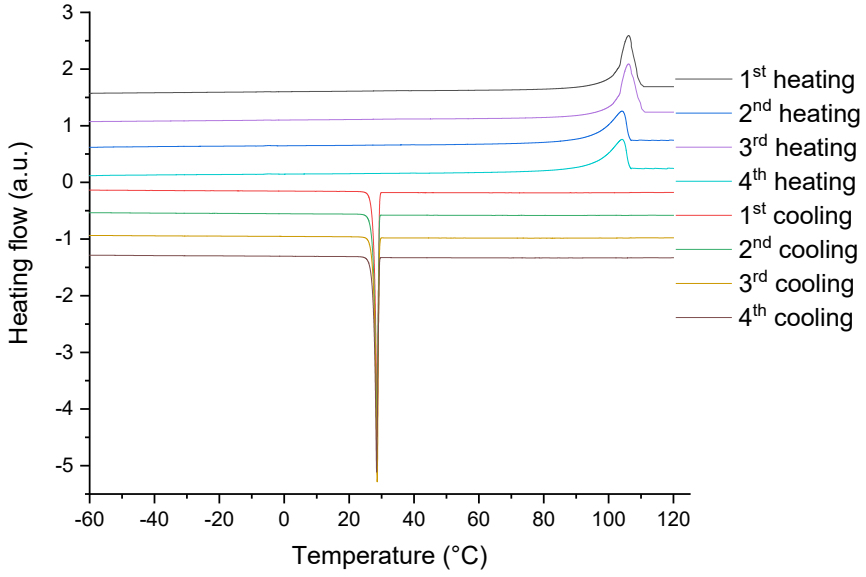

Figure S20: DSC traces of **2**.

The thermal trace of compound **2** reveals an endothermic phase transition at 97.0 °C upon first heating, corresponding to complete melting of the compound (Cr→Iso). This transition is reversed (Iso→Cr) upon cooling with crystallization at 29.8 °C. All subsequent thermal cycles exhibit the same two transitions, however, the melting temperature shifts increasingly towards lower temperature (96.7 °C for the fourth heating) and the shape of the endotherm becomes broader, while the recrystallization temperature stays the same over all cycles, exhibiting significant supercooling. The heat content stays unchanged (6.3 J/g upon heating; -6.1 J/g upon cooling).

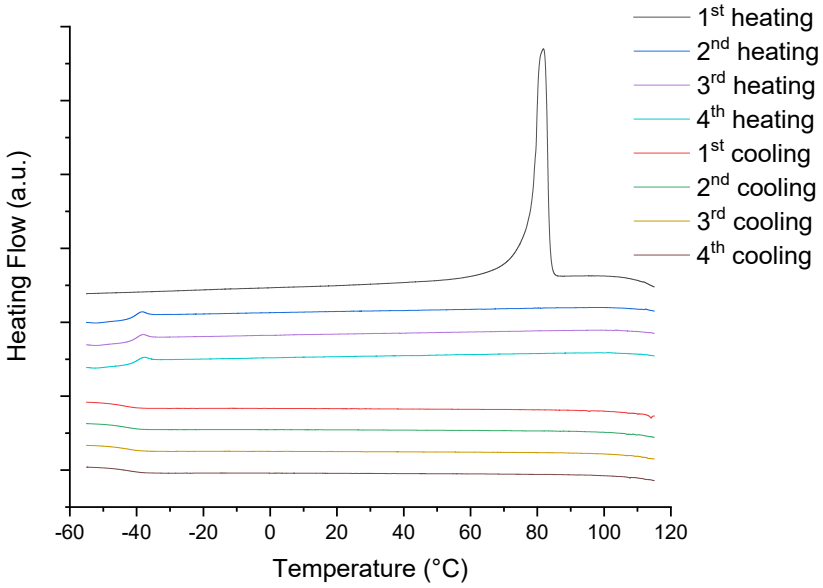

Figure S21: DSC traces of **3**.

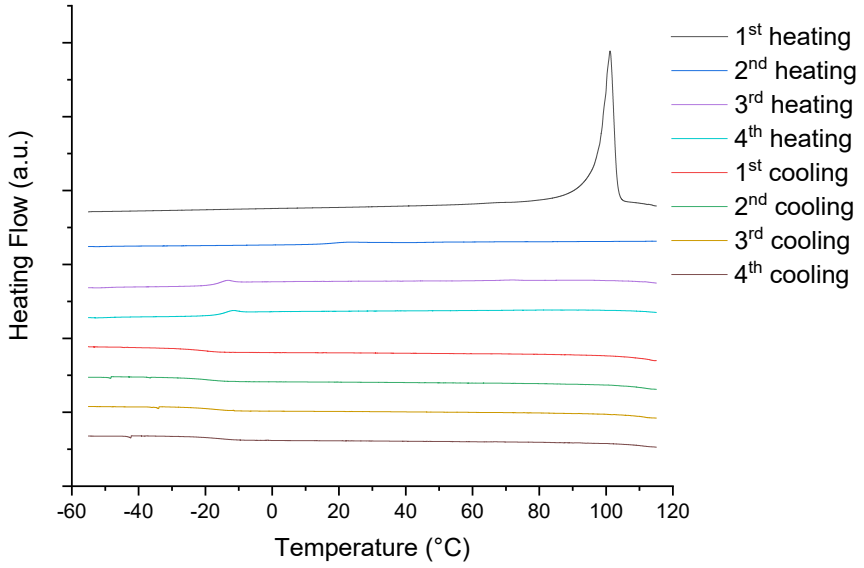

Figure S22: DSC traces of **4**.

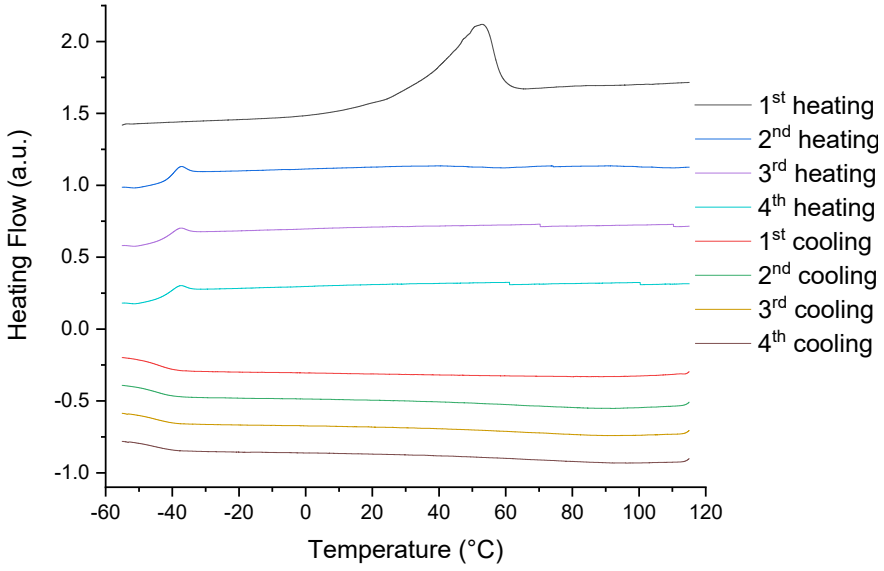

Figure S23: DSC traces of **5**.

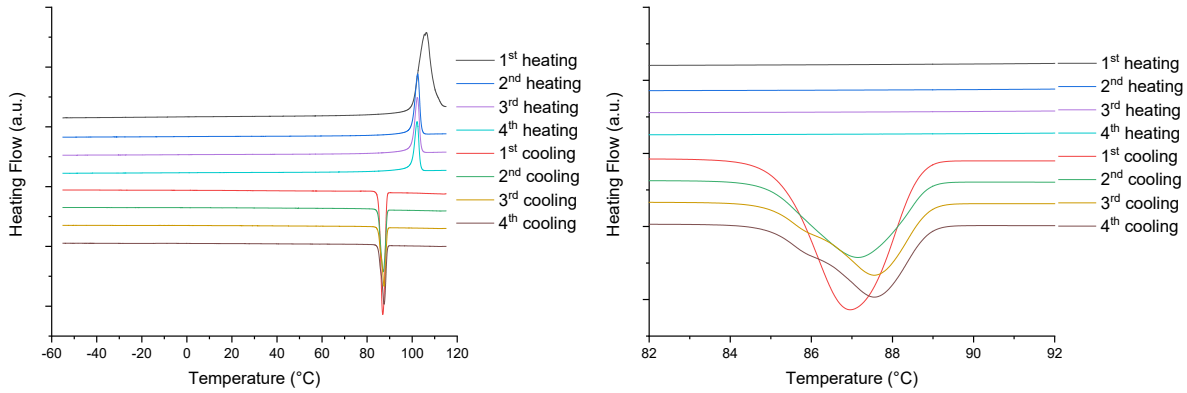

Figure S24: DSC traces of **6** (*left*) and zoomed in version of the exothermic peak (*right*).

For the first heating of **6**, an endothermic transition identified as the melting point (Cr→Iso) can be observed at 98.3 °C and a crystallization is observed on cooling at 89.9 °C (Iso→Cr). All following thermal cycles exhibit the two same transitions with a change on the sharpness of the melting transition and a progressive decrease of the intensity of both transitions (from 6.26/-6.28 J/g in the 1st run to 4.28/-4.25 J/g in the 4th).

All 6 salts exhibit thermal behavior commonly observed for ILs,[1] but each in its own way. **1** exhibits only a single reversible T_g, while **3-5** initially melt, but do not recrystallize within the parameters of the DSC experiment, with only a reversible T_g observed after the initial heating. **2** and **6** melt and then crystallize from the melt, however with significant different in the extent of supercooling (72.5 °C for **2** and 8.4 °C for **6**).

IV. Thermogravimetry Analysis (TGA) curves for 1-6

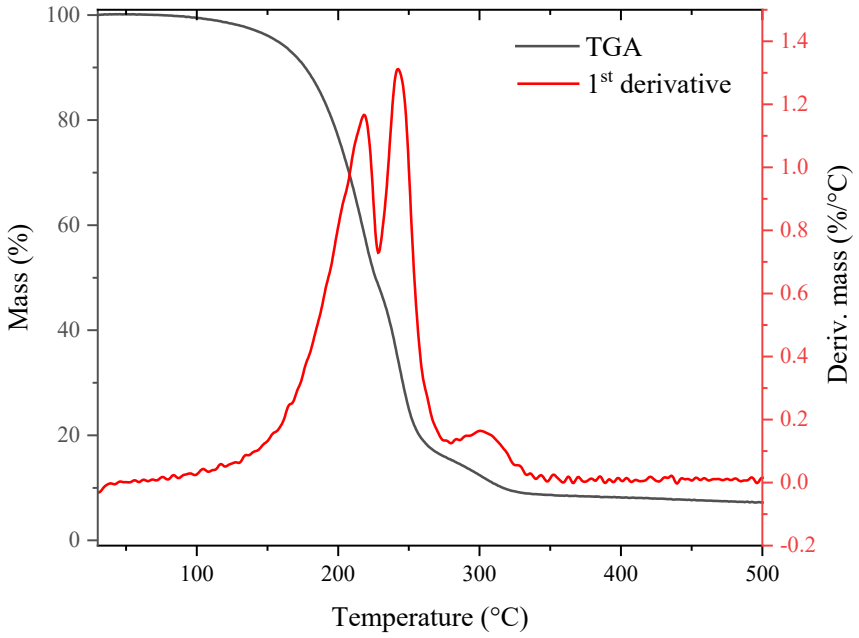

Figure S25: TGA curve of **1**.

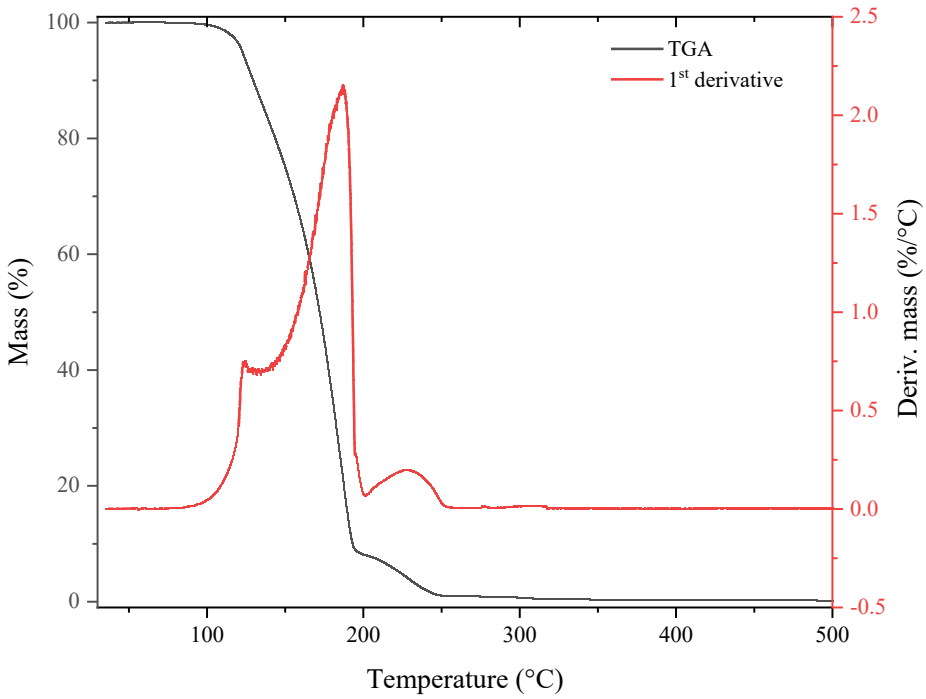

Figure S26: TGA curve of **2**.

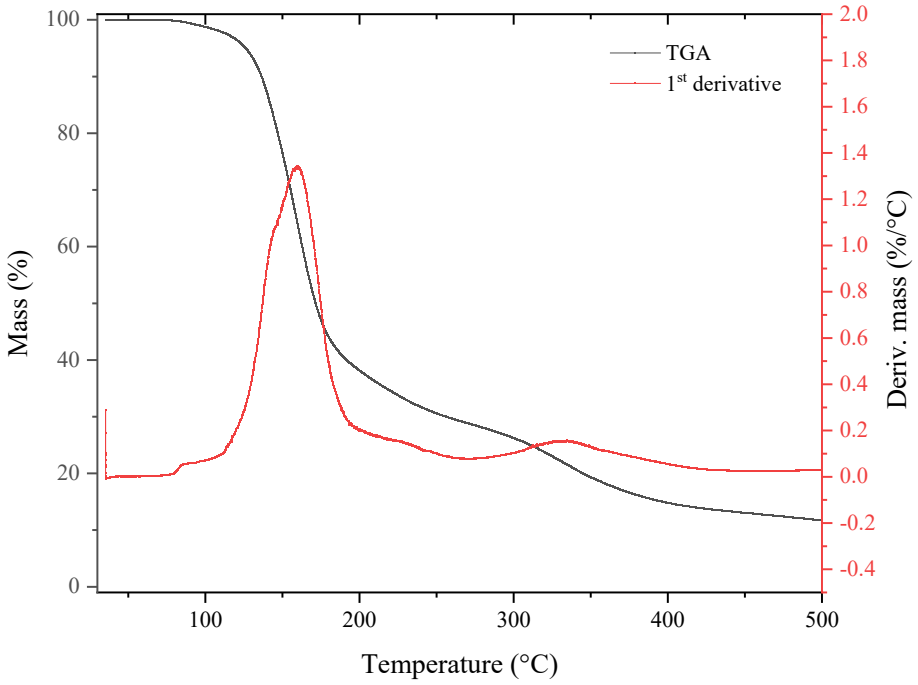

Figure S27: TGA curve of **3**.

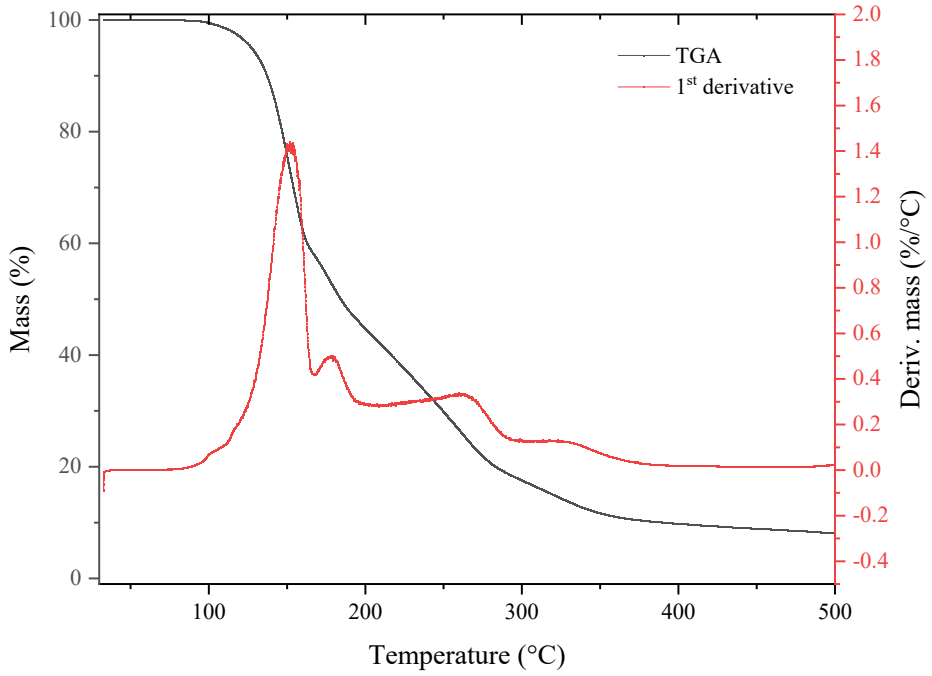

Figure S28: TGA curve of **4**, the first loss corresponds to a 43.83% mass loss.

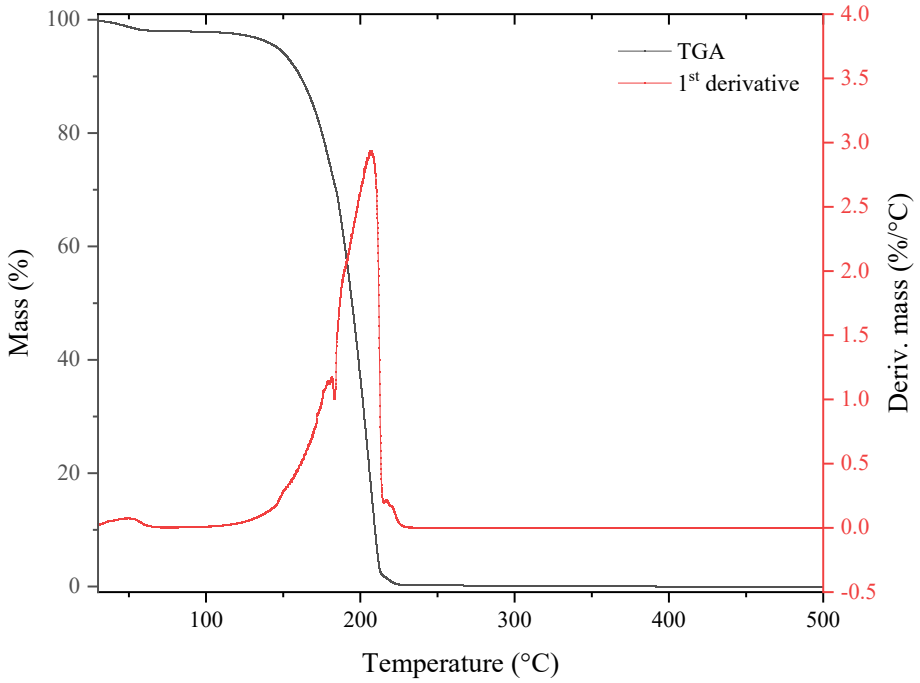

Figure S29: TGA curve of **5**.

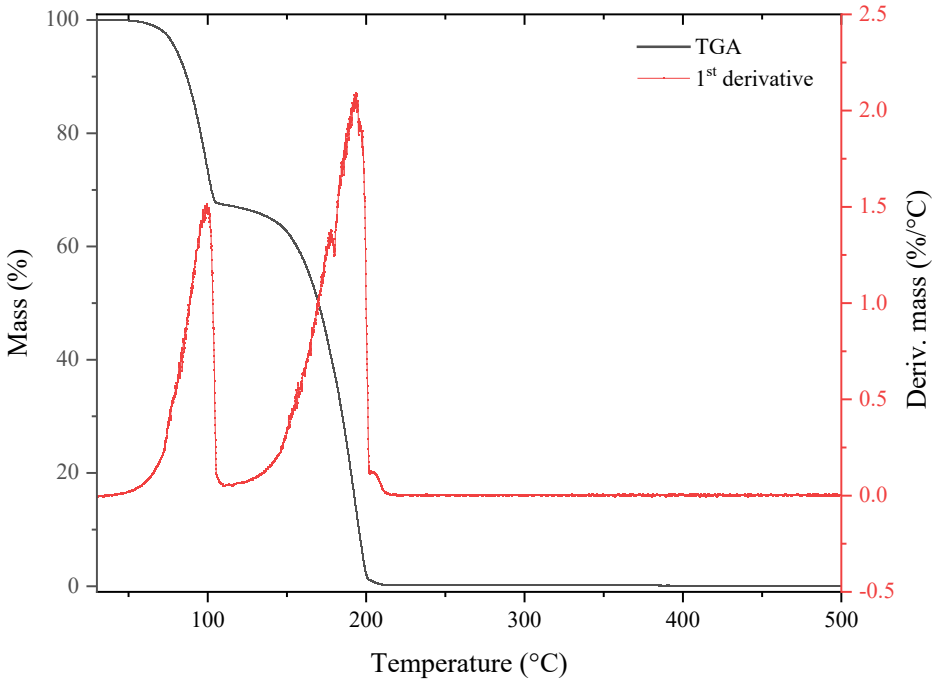

Figure S30: TGA curve of **6**, the first step corresponds to a 33.86% mass loss.

V. Polarized Optical Microscopy (POM) images

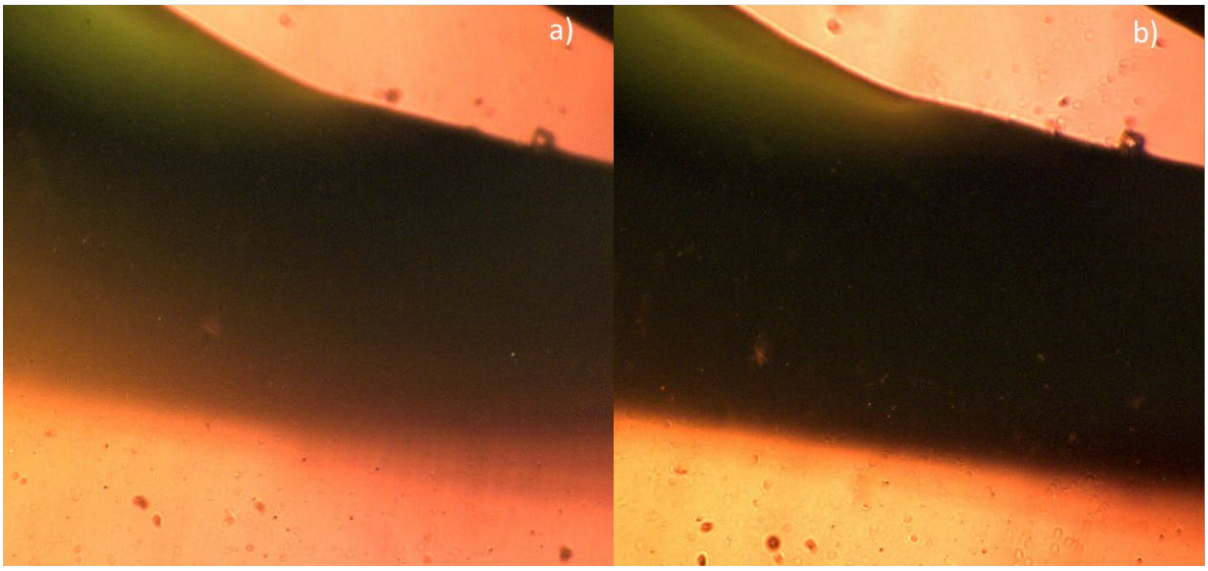

Figure S31: POM images of **1**: a) -170 °C (L_{iso}); b) 60 °C (L_{iso}).

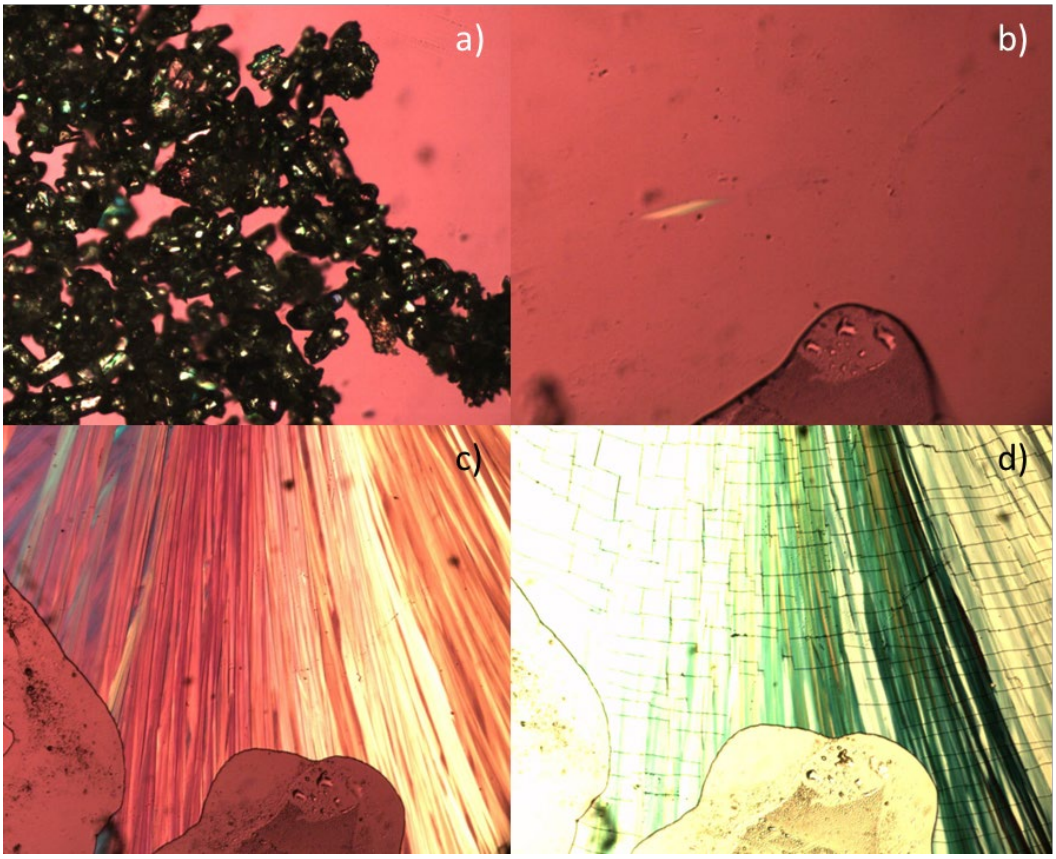

Figure S32: POM images of **2**: a) 70 °C upon heating (Cr); b) 110 °C upon heating (L_{iso}); c) 10 °C upon cooling (Cr); d) 10 °C upon cooling unpolarised (Cr).

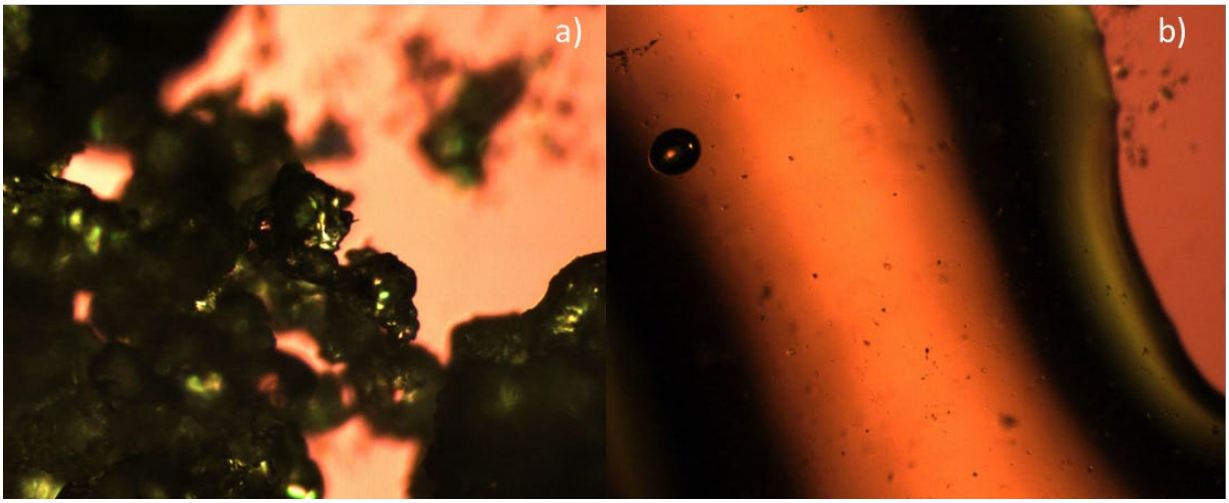

Figure S33: POM images of **3**: a) 40 °C (Cr); b) 90 °C (L_{iso}).

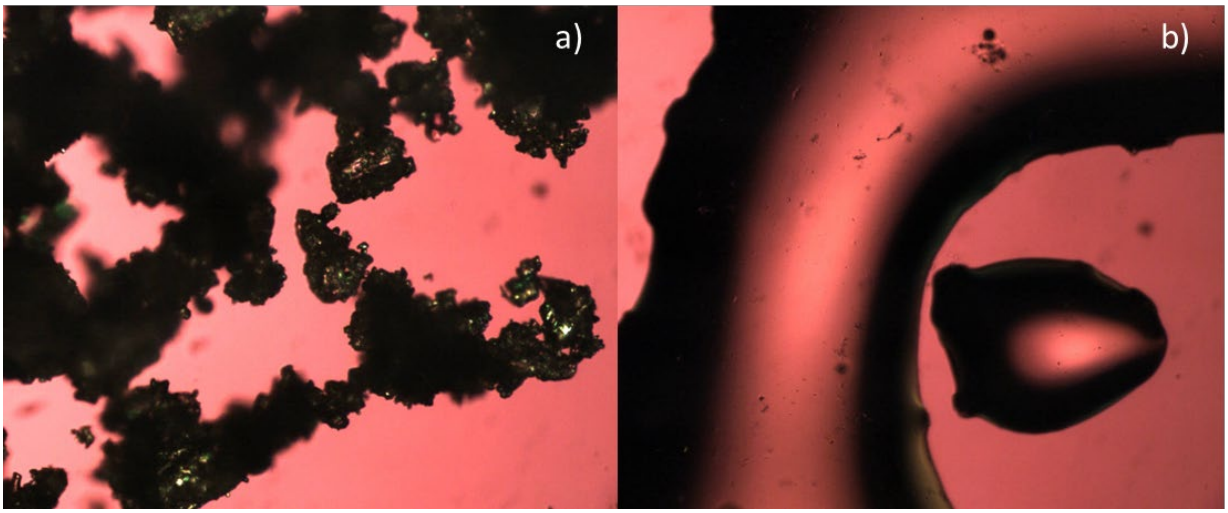

Figure S34: POM images of **4:** a) 70 °C (Cr); b) 110 °C (L_{iso}).

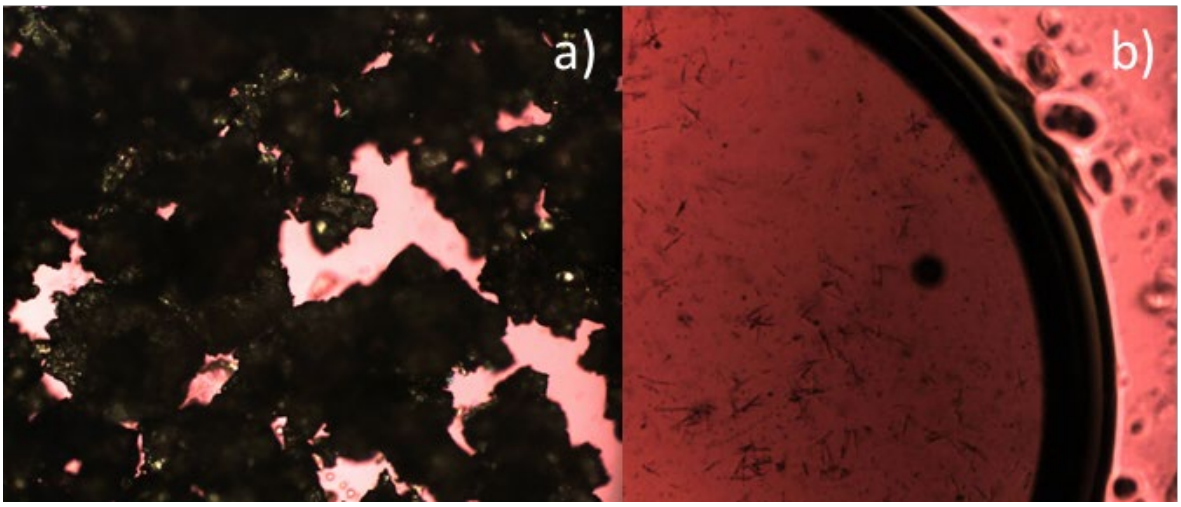

Figure S35: POM images of **5**: a) 25 °C (Cr); b) 45 °C upon heating (L_{iso}).

Figure S36: POM images of **6**: a) 80 °C upon heating (Cr); b) 105 °C upon heating (L_{iso}); c) 84 °C upon cooling (recrystallization → Cr).

VI. Structural data

Table S1. Interatomic angles in the azole rings of **2-6** expressed in degrees (°).

	2	**3**	**4**	**5**	**6**	**6'**	
∠N2-C2-N5	105(1)	107.4(2)	105.4(4)	88.8(1)	88.0(2)	88.4(2)	∠C1-S1-C2
∠C2-N5-N4	111(1)	109.0(2)	109.8(4)	113.2(1)	113.8(4)	114.2(4)	∠S1-C2-N2
∠N5-N4-N3	104(1)	105.1(2)	106.0(4)	113.0(1)	112.6(4)	111.9(4)	∠C2-N2-N3
∠N4-N3-C2	112(1)	114.1(3)	110.8(4)	114.4(1)	113.8(4)	115.0(4)	∠N2-N3-C1
∠N3-C2-N5	107(1)	104.3(2)	107.9(4)	110.6(1)	111.8(3)	110.4(3)	∠N3-C1-S1

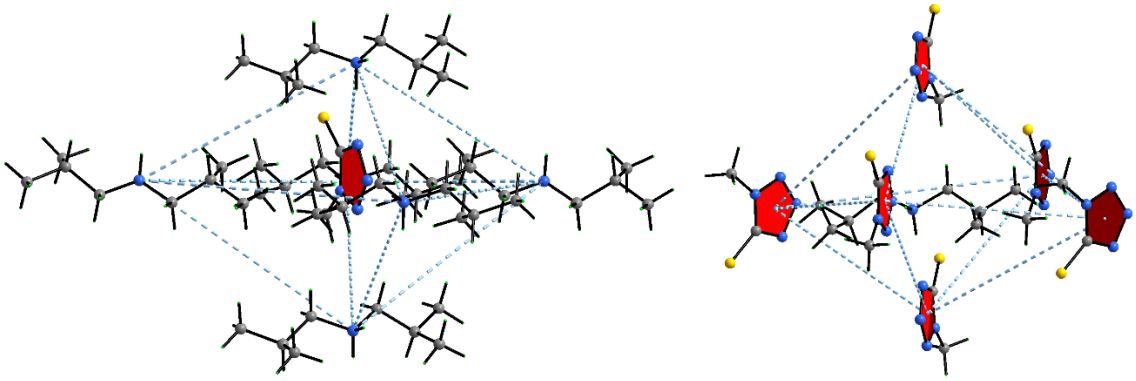

Figure S37. Octahedral coordination of the anion and the cation in the crystal structure of **2**.

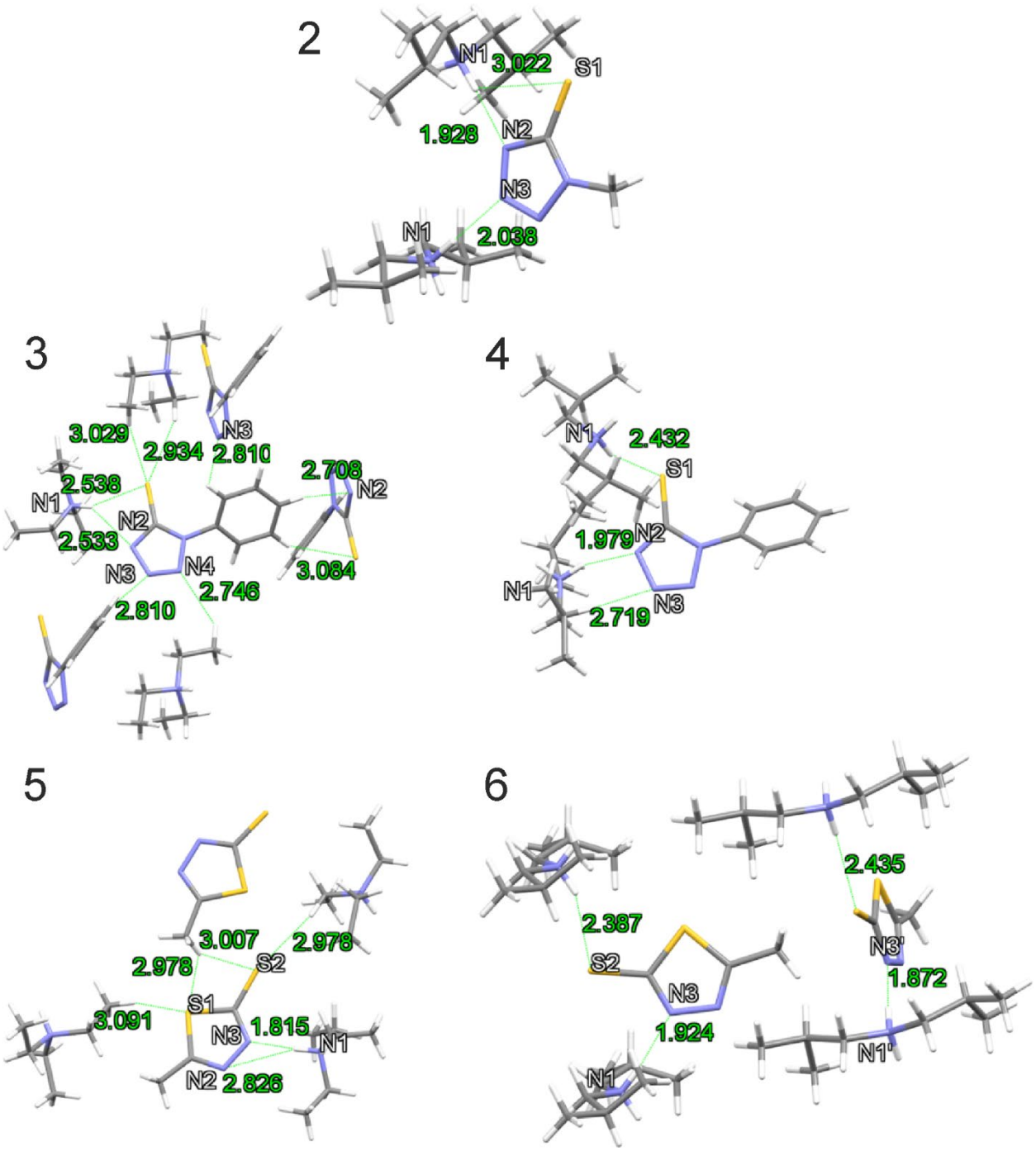

Figure S38. Close contacts (Å) for **2**-**6**.

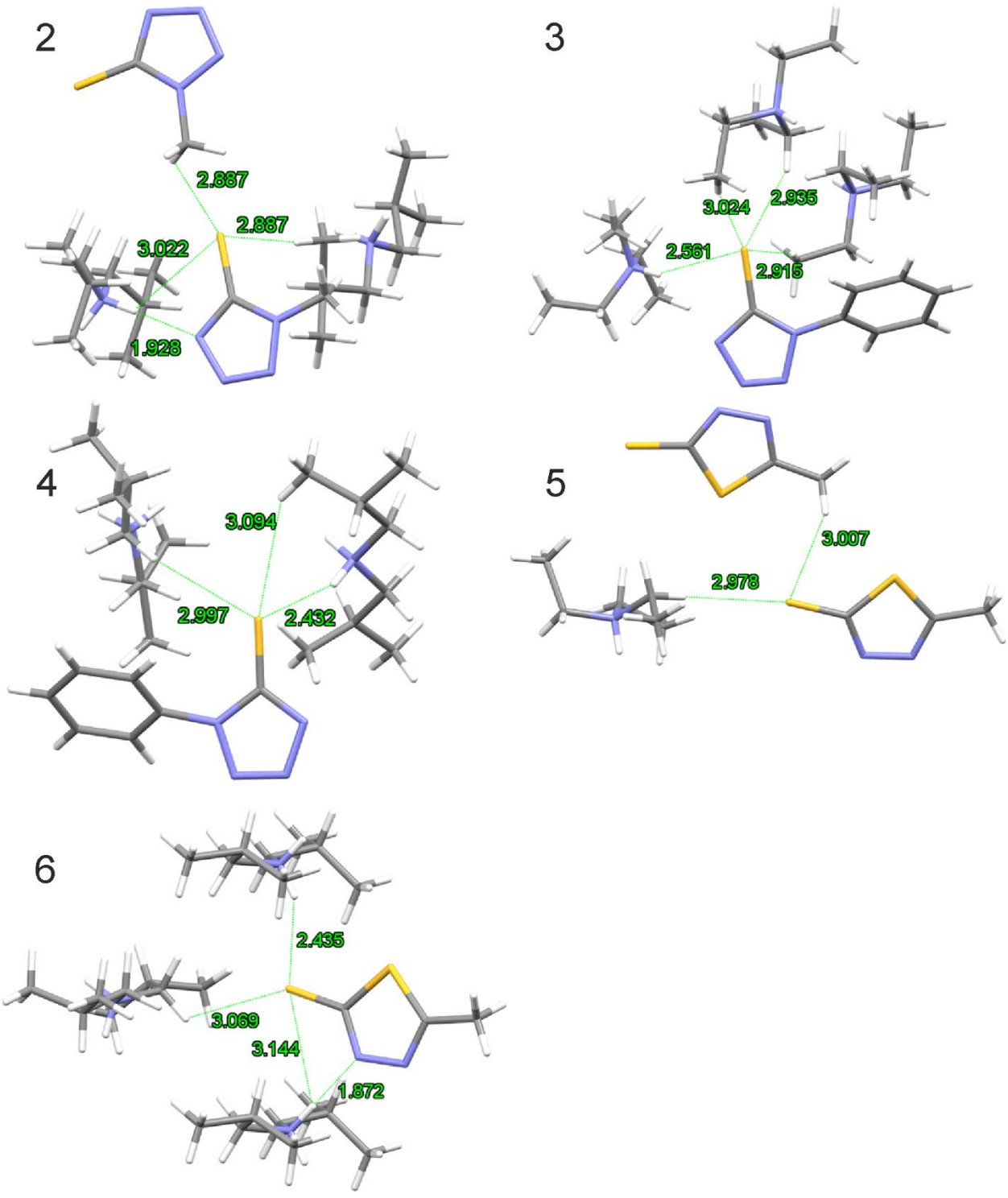

Figure S39. S···H hydrogen bonds (Å) in **2-6**. The most important hydrogen-bonds are depicted with green dotted lines.

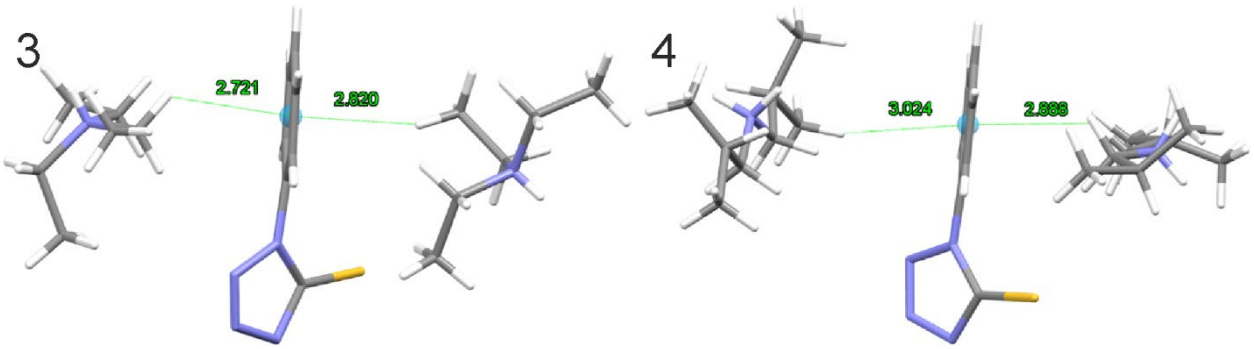

Figure S40. Most important short contacts and hydrogen-bonds (Å) from and to the phenyl moiety in **3** and **4**.

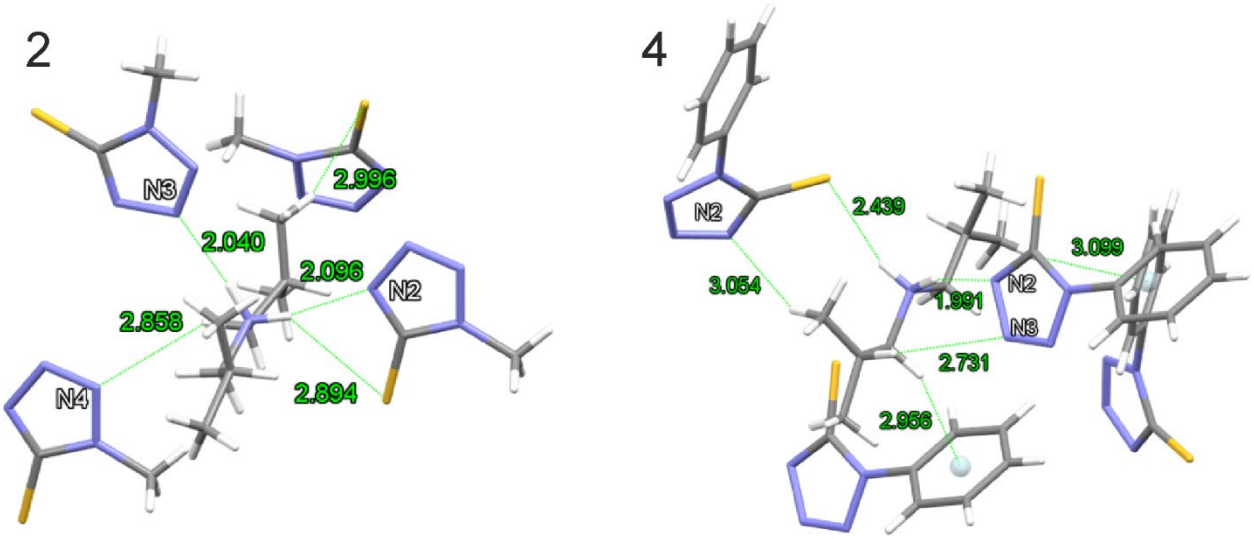

Figure S41. Main hydrogen-bonds and close contacts (Å) in **2** and **4**.

VII. Powder X-Ray Diffraction (PXRD) diffractograms for 2-6

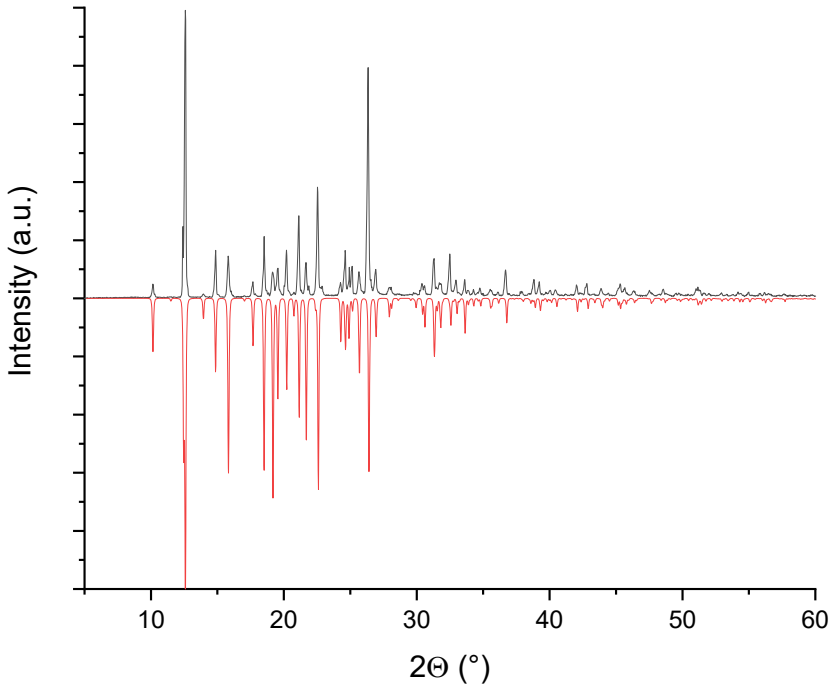

Figure S42: PXRD diffractogram of **2** (black trace) vs. theoretical diffractogram (red trace).

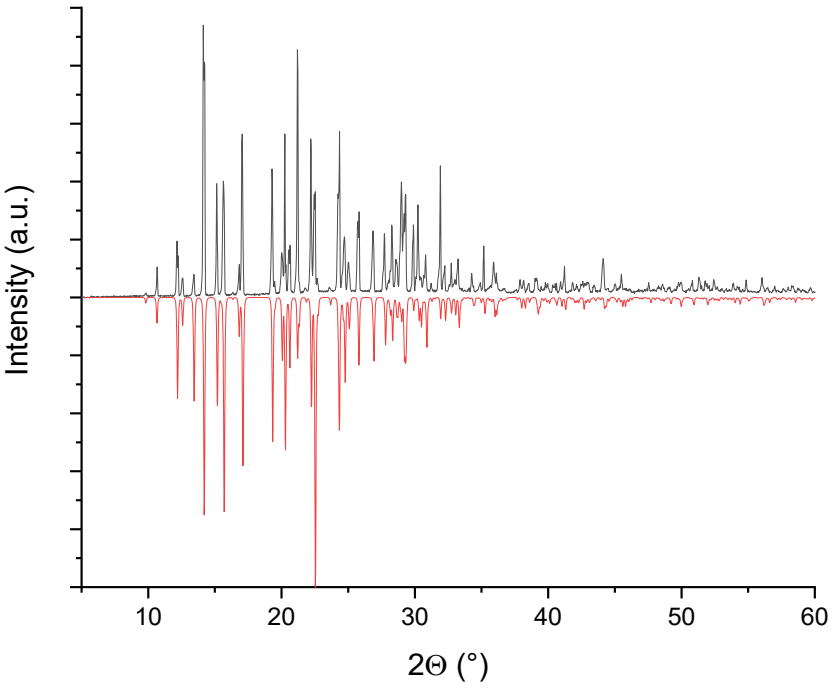

Figure S43: PXRD diffractogram of **3** (black trace) vs. theoretical diffractogram (red trace).

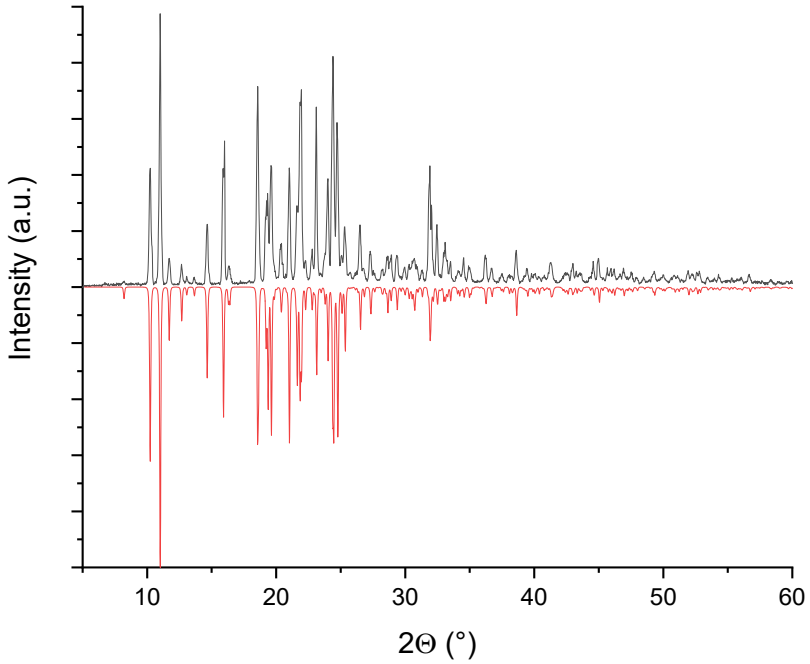

Figure S44: PXRD diffractogram of **4** (black trace) vs. theoretical diffractogram (red trace).

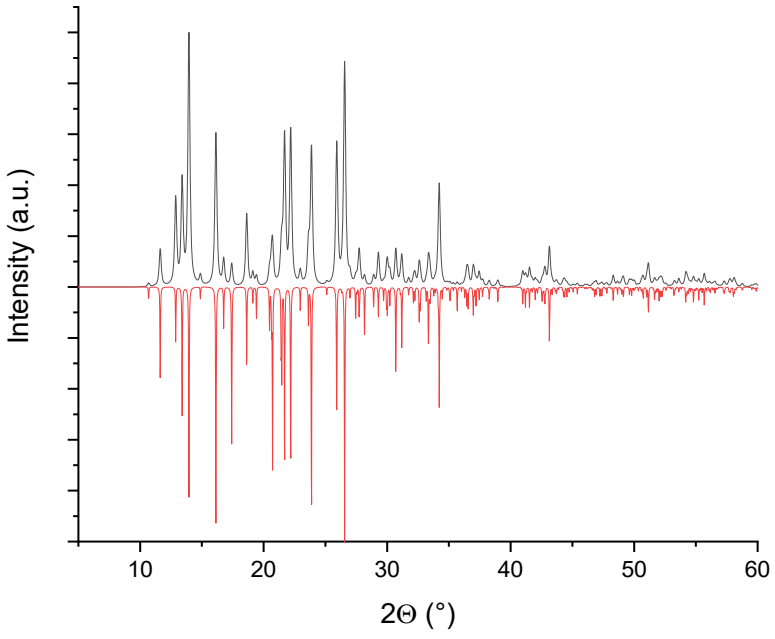

Figure S45: PXRD diffractogram of **5** (black trace) vs. theoretical diffractogram (red trace).

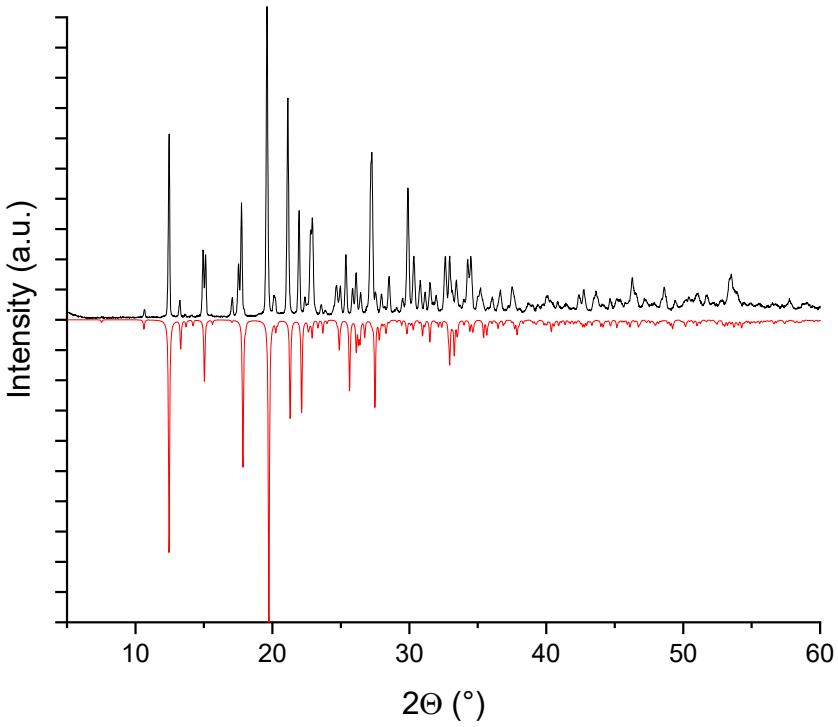

Figure S46: PXRD diffractogram of **6** (black trace) vs. theoretical diffractogram (red trace).

VIII. Hirshfeld surface analysis details

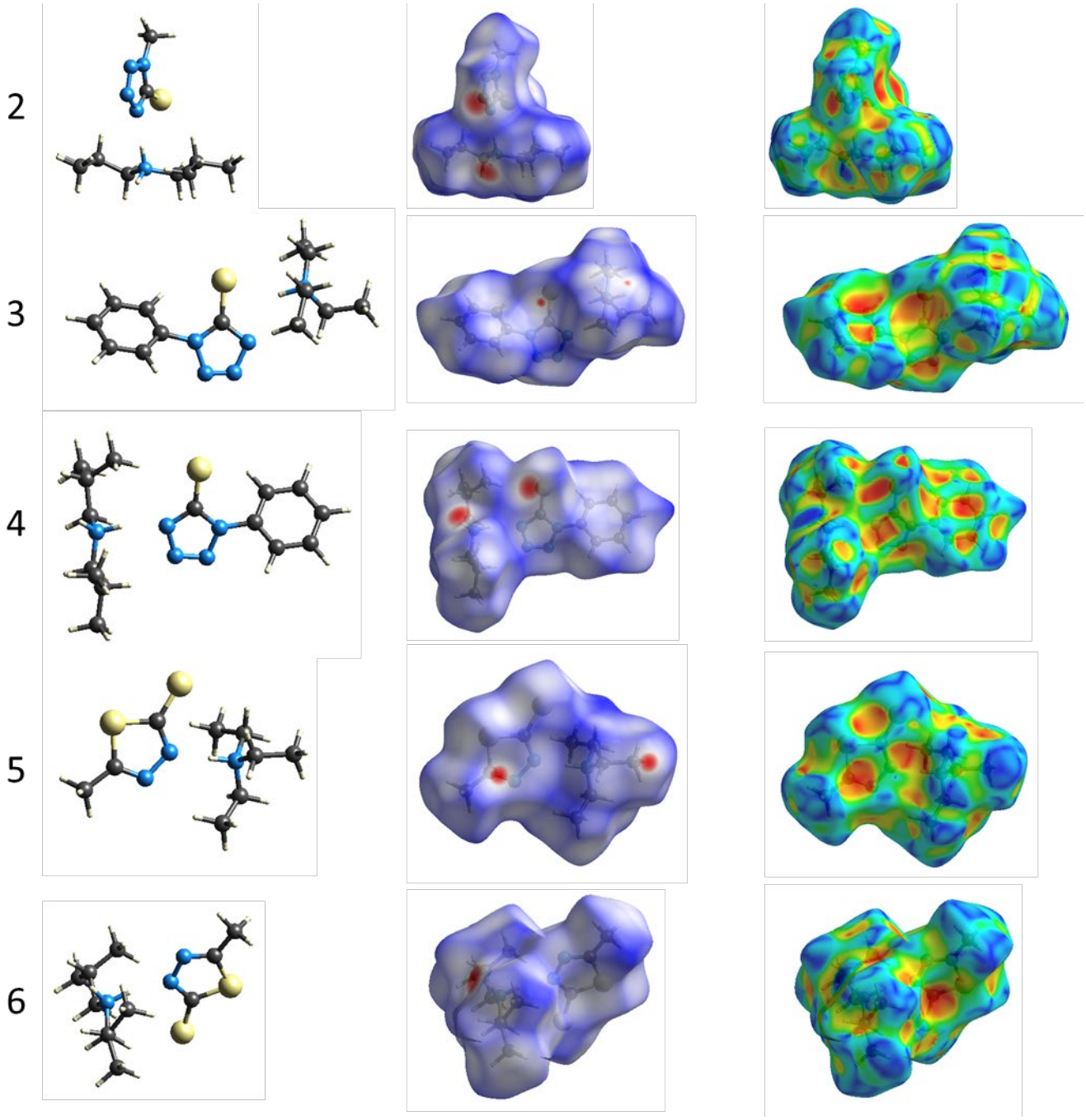

Figure S47: Cation anion pair for each (*left*), the molecules with the Hirshfeld surfaces mapped with d_{norm} (*middle*) and the shape index (*right*).

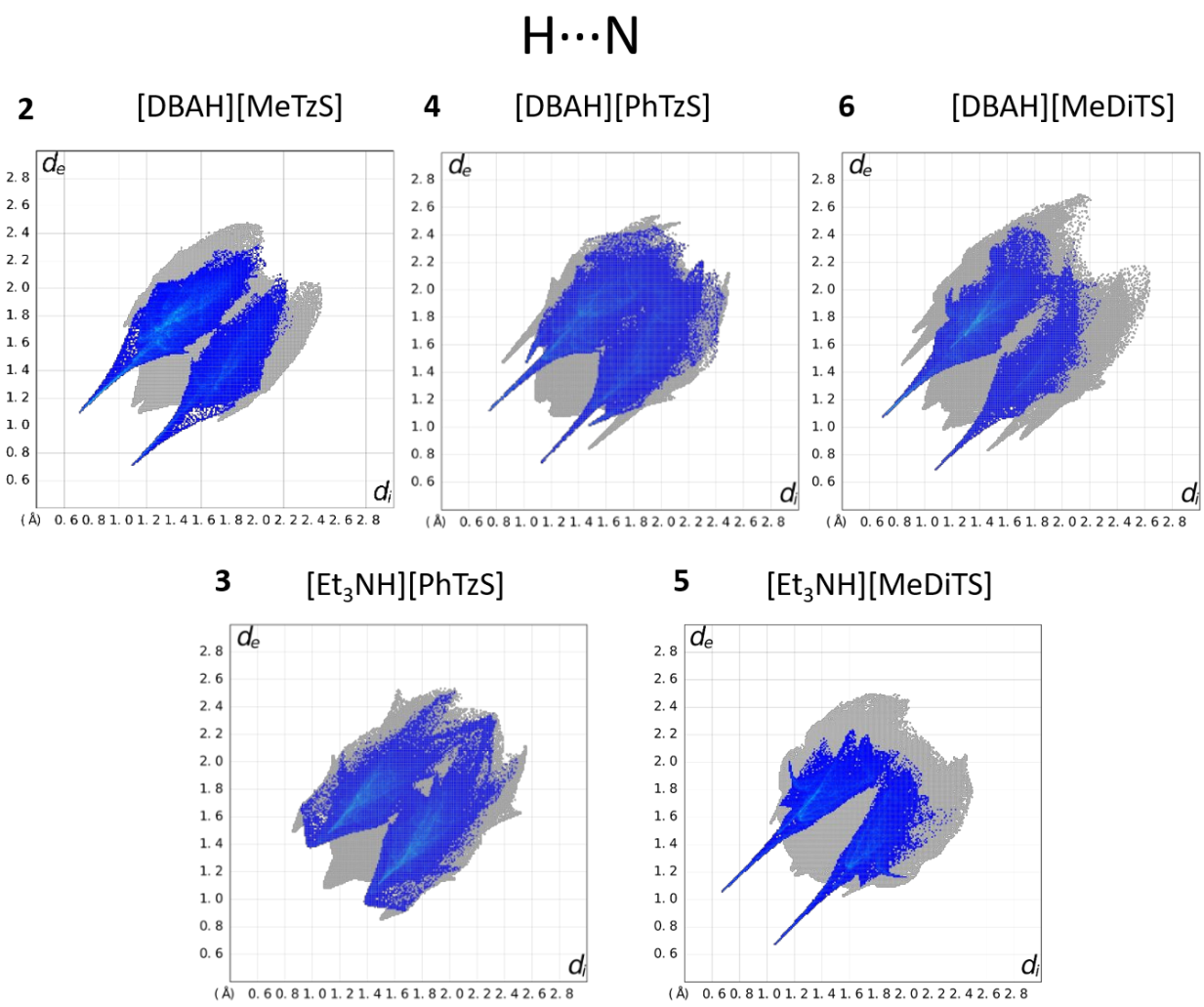

Figure S48: Highlighted H···N interactions on the fingerprint plot of **2-6**.

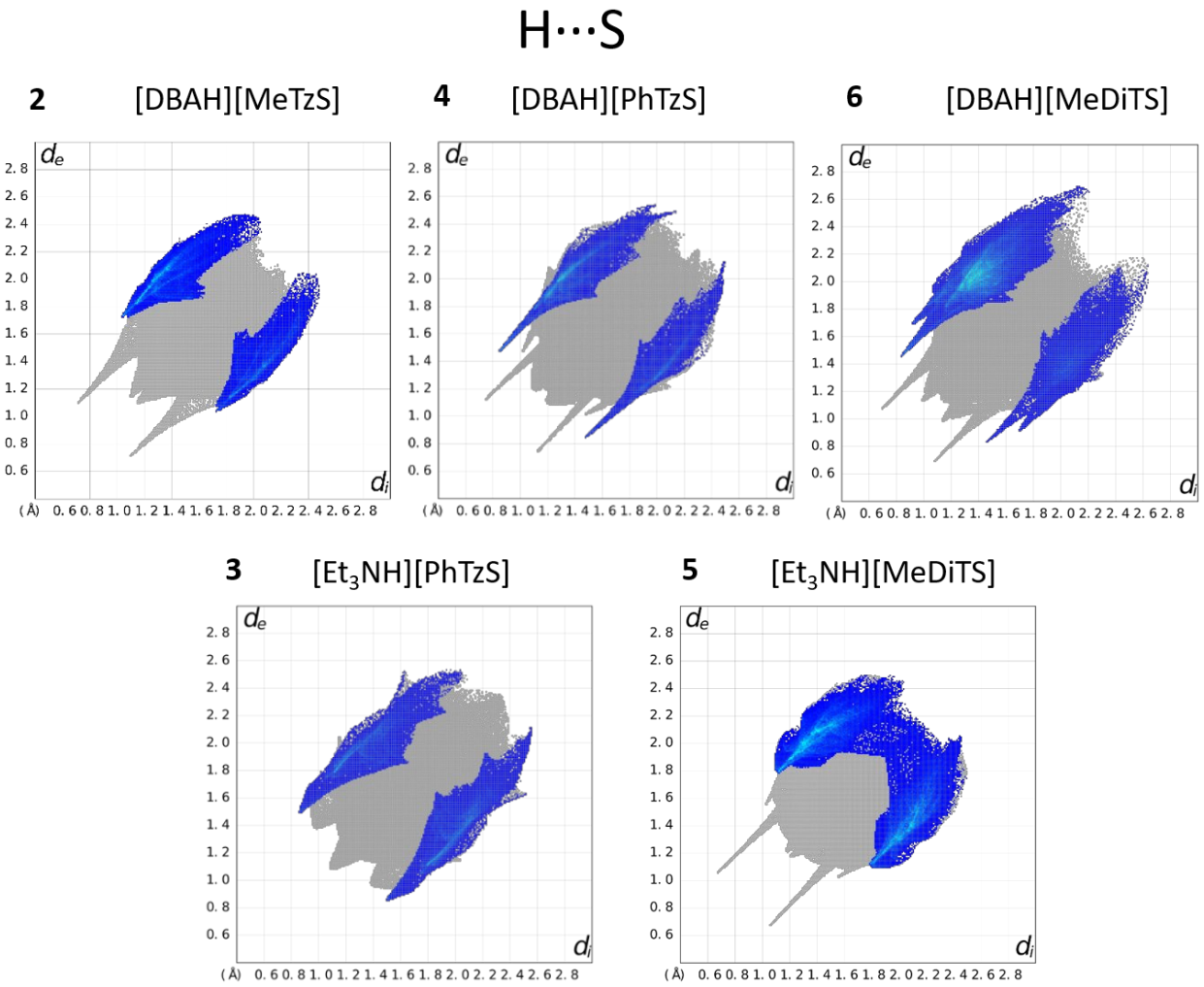

Figure S49: Highlighted H···S interactions on the fingerprint plot of **2-6**.

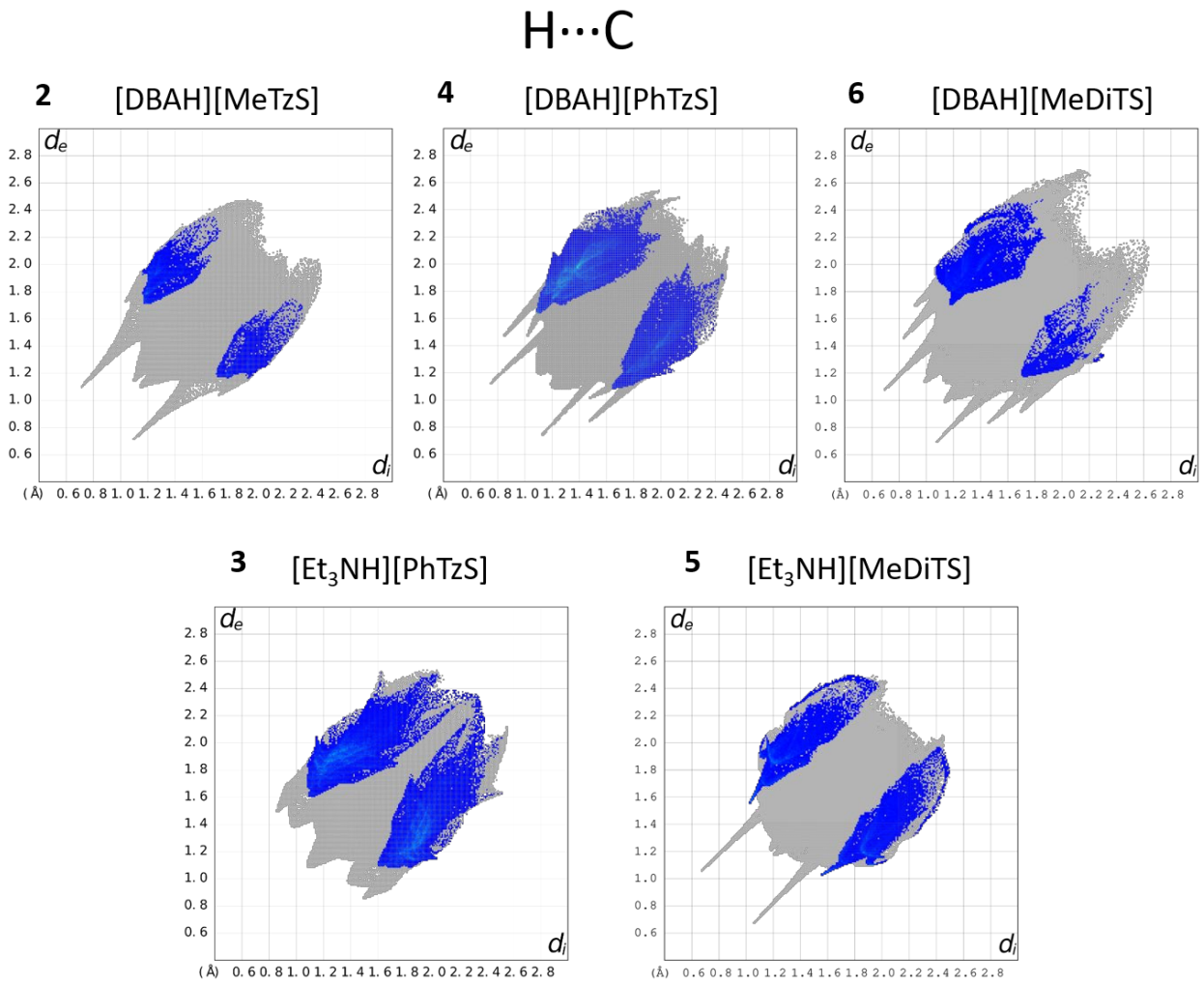

Figure S50: Highlighted H···C interactions (mainly responsible for C-H···π interactions) on the fingerprint plot of **2-6**.

Table S2: Percentages of interactions between atoms in the solid state.

	H···All	H···N	H···S	H···C	H···H
2	85.3	22.6	14.3	2.7	60.4
3	72.8	22.5	14.3	15.3	47.9
4	83.1	20.8	12.4	13.7	53.1
5	76.0	14.4	27.6	6.5	51.5
6	90.6	14.8	25.2	2.7	57.3

IX. References

1. Renier, O.; Bousrez, G.; Yang, M.; Hölter, M.; Mallick, B.; Smetana, V.; Mudring, A.-V., Developing design tools for introducing and tuning structural order in ionic liquids. *CrystEngComm* **2021,** *23* (8), 1785-1795.